mining

MDPI

Article

Field-Validated Multisensor Assessment of Haul-Road Degradation and Its Association with Fuel-Use Proxy Burden, Dynamic Response, and Transport-Cycle Stability in Open-Pit Mining

Shakenov Aman Tulegenovich [1], Utegenova Assem Yerzhankyzy [1,*], Stolpovskikh Ivan Nikitovich [1], Orumbassarova Ainura Berikbolovna [1], Boris V. Malozyomov [2] and Nikita V. Martyushev [3,*]

[1] Institute of Energy and Mechanical Engineering Named After A. Burkitbayev, Department of Technological Machines and Gas Turbine Installations, Satbayev University, Almaty 050013, Kazakhstan; ashakenov@yahoo.com (S.A.T.); i.stolpovskikh@satbayev.university (S.I.N.); a.orumbassarova@satbayev.university (O.A.B.)

[2] Department of Electrotechnical Complexes, Novosibirsk State Technical University, 20, Karla Marksa Ave., 630073 Novosibirsk, Russia; borisnovel@mail.ru

[3] Department of Information Technologies, Tomsk Polytechnic University, 634050 Tomsk, Russia

* Correspondence: a.utegenova@satbayev.university (U.A.Y.); martjushev@tpu.ru (N.V.M.)

Abstract

The performance of haul trucks in open-pit mining is strongly affected by haul-road geometry, surface condition, rolling resistance, and operational traffic regimes. However, existing studies often consider road-surface mapping, vehicle dynamic response, and onboard telemetry as separate information streams, which limits the reproducible assessment of how road-related factors are associated with VIMS-derived fuel-use proxy burden, mechanical dynamic response, and transport-cycle instability. This study proposes a field-based, segment-level multisensor framework that integrates unmanned aerial vehicle/light detection and ranging (UAV/LiDAR) road-surface reconstruction, global positioning system/inertial measurement unit (GPS/IMU) trajectory and vibration data, and Caterpillar Vial Information Management System (VIMS) telemetry into a unified spatiotemporal analytical dataset. The methodological contribution consists in the synchronization of heterogeneous data sources at the road-segment level, the calculation of interpretable road-condition and vehicle-response indicators, and the statistical assessment of road-related effects while explicitly accounting for confounding factors such as longitudinal grade, payload state, speed regime, truck class, and operational variability. Unlike studies that use LiDAR mapping, vibration monitoring, or onboard telemetry as separate diagnostic channels, the proposed approach introduces a segment-level analytical framework in which road morphology, truck response, and operational penalties are aligned within the same spatial unit, interpreted under confounder-aware conditions, and verified through repeat-pass reproducibility and robustness checks. The framework was tested on haul roads around the Ekibastuz open-pit coal mine. The field analysis identifies road segments where degraded surface morphology, increased waviness, unfavorable longitudinal profile, and higher rolling resistance coincide with increased mechanical dynamic response, VIMS-derived fuel-use proxy burden, braking instability, and travel-time variability. The results are interpreted as controlled field-supported associations rather than as isolated causal effects. The proposed maintenance ranking should therefore be regarded as a decision-support output, while the operational effectiveness of specific repair interventions requires future before–after validation.

Check for updates

Academic Editor: Marilena Cardu

Received: 2 June 2026
Revised: 27 June 2026
Accepted: 2 July 2026
Published: 5 July 2026

Copyright: © 2026 by the authors. Licensee MDPI, Basel, Switzerland. This article is an open access article distributed under the terms and conditions of the Creative Commons Attribution (CC BY) license.

Keywords: open-pit mining; haul roads; haul-road degradation; haul trucks; multisensor monitoring; unmanned aerial vehicle LiDAR; global positioning system; inertial measurement unit; Vital Information Management System; dynamic load response; fuel-use proxy burden; transport-cycle stability; maintenance prioritization

1. Introduction

The efficiency of transport processes in open-pit mining depends not only on haul-truck capacity and operating mode, but also on the actual condition of intra-pit haul roads [1–3]. In cyclic haulage systems, the road acts as a functional link between the designed transport scheme and its real production performance.

Deterioration of the haul-road profile, increased roughness, waviness, rutting, and local surface defects can increase rolling resistance, destabilize the speed regime, intensify dynamic loading of the vehicle, and reduce the stability of the transport cycle [4,5]. For this reason, haul-road condition should be considered not as an auxiliary infrastructure characteristic, but as a controllable factor of energy efficiency, equipment loading, and production stability in open-pit transport systems [6,7].

Existing approaches to haul-road assessment can be grouped into three main directions. The first direction focuses on direct inspection of the roadway and includes visual inspection, geodetic measurements, profiling, and remote sensing [8,9]. These methods provide information on road geometry and visible defects, but they do not directly quantify the vehicle response or operational consequences of degradation.

The second direction is based on vehicle-response monitoring using GPS, IMU, and vibration data [10,11]. These data make it possible to identify changes in speed regime, vertical acceleration, braking instability, and traffic irregularity. However, when used alone, vehicle-response data do not always explain whether the recorded response is caused by surface degradation, longitudinal grade, curvature, payload state, or operating regime.

The third direction considers the energy and operational consequences of haul-road deterioration, including increased rolling resistance, higher fuel demand, lower productivity, and accelerated mechanical loading of chassis and suspension components. Despite the practical value of these approaches, they are often applied separately. As a result, road geometry, road-surface condition, truck response, and operational penalties remain insufficiently connected within a single analytical framework [12].

This limitation is especially important for operational road management. A segment may appear geometrically unfavorable but produce only a moderate vehicle response, whereas another segment with less visually pronounced defects may generate increased braking, vertical acceleration peaks, suspension-pressure variability, and fuel-related burden [13]. Therefore, the assessment should move from isolated defect description to a segment-level interpretation in which road-surface condition, geometric burden, vehicle response, and operational consequences are analyzed jointly. This logic makes it possible to identify haul-road segments that are critical for energy use, mechanical loading, transport-cycle stability, and maintenance prioritization [14].

In recent years, interest in this problem has increased due to the development of unmanned aerial vehicle/light detection and ranging (UAV/LiDAR) scanning, mobile inertial measurement unit (IMU) systems, onboard telemetry of heavy equipment, and digital operation-support tools. Work on the assessment of haul-road rolling resistance, energy losses in the open-pit haulage system, analysis of the vibration signature of roads, and the use of UAVs for monitoring the condition of the pavement have shown that road infrastructure has a direct impact on the efficiency of haulage operations [15]. However, even

with such studies, a field-verified integrated methodology is relatively rarely formed, in which data of different modalities are synchronized in a single spatiotemporal contour and are used to construct quantitative indicators that simultaneously reflect the morphological degradation of the road, the dynamic response of the vehicle and operational losses [16]. As a result, digital monitoring tools often remain either at the level of defect mapping or at the level of recording machine behavior, without moving on to the task of direct engineering prioritization of segments according to the degree of their actual production damage [17].

This study is aimed at eliminating this gap using the example of intra-pit technological roads around the Ekibastuz coal deposit. The choice of this object is due to a combination of several factors: the high intensity of heavy dump truck traffic, the variability of the longitudinal profile, the presence of curvilinear sections, and local zones of undulation and defectiveness of the pavement, as well as the pronounced sensitivity of transport indicators to the quality of the road [18]. Such an operational environment makes it possible to analyze road degradation not in an abstract form, but as a real factor that simultaneously affects the kinematics of traffic, the dynamic load of the vehicle and the energy efficiency of the transport process. In this regard, the aim of this study is to quantify field-supported associations between segment-level haul-road degradation and haul-truck mechanical dynamic response, VIMS-derived fuel-use proxy burden, and transport-cycle instability based on synchronized UAV/LiDAR, GPS/IMU, and VIMS data [19].

To achieve this aim, the present study performs four specific tasks. First, it constructs a field dataset combining UAV/LiDAR road-surface reconstruction, global positioning system/inertial measurement unit (GPS/IMU) motion records, and Vital Information Management System (VIMS) telemetry for repeated truck passes. Second, it converts these heterogeneous measurements into segment-level observations using a common spatial reference and synchronized passage intervals [20]. Third, it calculates derived indicators describing road condition, mechanical dynamic response, VIMS-derived fuel-use proxy burden, braking instability, and grade severity. Fourth, it ranks haul-road segments according to their measured operational criticality. Previous studies are used to define the research gap, whereas the methodological and analytical sections of this paper focus on the field dataset collected in this study, synchronization procedure, indicator calculation, and segment-level interpretation [21].

To address this gap, the study develops a segment-level field methodology in which road-surface morphology, vehicle kinematics, inertial response, and onboard operational telemetry are aligned within the same spatial units. Unlike LiDAR-only road-condition mapping or vibration-only ride-quality assessment, the proposed framework treats the haul road as a coupled road–vehicle–operation system. The main contribution is therefore not the use of several sensors as such, but the construction of a reproducible analytical chain from heterogeneous field measurements to segment-level indicators, confounder-aware interpretation, and maintenance-oriented ranking of haul-road sections.

The novelty of the proposed framework is expressed in four methodological elements. First, heterogeneous LiDAR, GPS/IMU, and VIMS records are not merely combined, but converted into a common observation unit defined as one truck pass through one road segment. Second, the framework separates road-surface descriptors from geometric and resistance-related covariates, including grade, rolling resistance, and curvature, which reduces the risk of attributing all operational variation to surface degradation alone. Third, the derived indicators are used not only for descriptive monitoring, but also for confounder-aware regression modelling of dynamic response, fuel-related penalty, and transport-cycle instability. Fourth, the ranking of critical segments is verified through repeat-pass reproducibility, bootstrap resampling, repeated subsampling, and leave-one-route-out validation. Thus, the contribution of the study is a validated segment-level analytical

framework for haul-road condition assessment rather than a simple integration of several monitoring technologies.

Figure 1 provides a technical overview of the analytical framework used in this study. The figure is placed at the end of the Introduction to clarify the methodological logic of the study before the detailed field-data description. It shows how UAV/LiDAR, GPS/IMU, and VIMS measurements are converted into synchronized segment-level observations and then used for indicator calculation, statistical modelling, validation, and confounder-aware engineering interpretation. The diagram is presented as a technical workflow scheme. Each block corresponds to a reproducible methodological operation used in the subsequent sections, and the arrows indicate the sequential direction of data processing rather than physical causation.

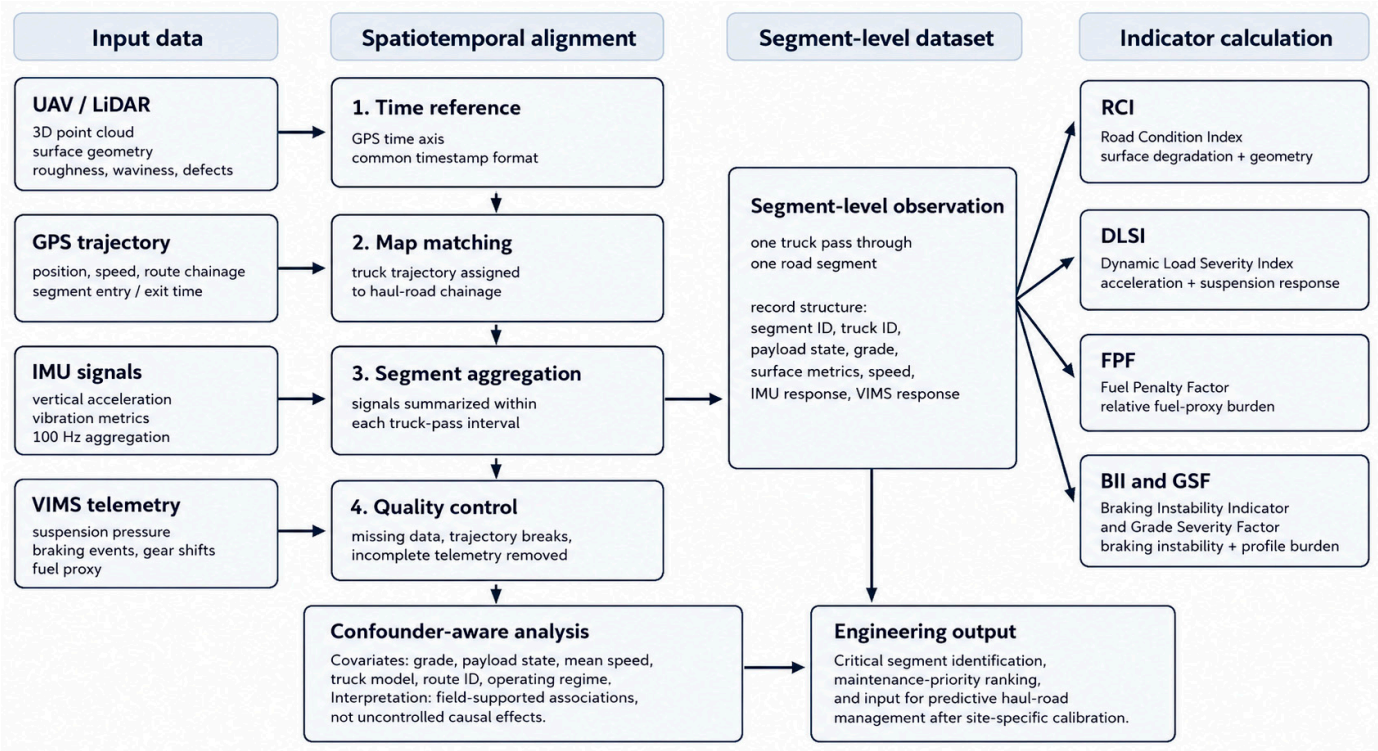


Figure 1. Segment-level multisensor framework for haul-road condition assessment. The technical workflow shows the transformation of UAV/LiDAR, GPS/IMU, and VIMS measurements into synchronized segment-level observations, followed by indicator calculation, statistical modelling, validation, and confounder-aware engineering interpretation. Arrows denote the sequential data-processing flow between labelled methodological blocks.

The workflow arrows should not be interpreted as proof of a physical causal chain. They indicate the sequence of data processing, synchronization, indicator calculation, validation, and engineering interpretation. Causal confirmation would require a separate intervention-based or before–after maintenance design.

In Figure 1, the arrows are used in a single technical sense: they show the movement of data from input measurements to spatiotemporal alignment, segment-level aggregation, indicator calculation, and engineering interpretation. They do not represent separate physical causal mechanisms. The central block is labelled as the segment-level observation dataset, which forms the methodological link between raw multisensor records and subsequent statistical analysis.

The proposed workflow begins with four input data streams: UAV/LiDAR-based road-surface reconstruction, GPS trajectory records, IMU dynamic-response signals, and VIMS onboard telemetry. These data sources differ in sampling frequency, spatial resolution,

and physical meaning; therefore, they are first converted into a common spatiotemporal representation. GPS time is used as the reference temporal axis, while road chainage is used as the spatial reference for assigning truck passes to specific haul-road segments.

After synchronization and quality control, each analytical observation corresponds to one truck passage through one road segment. This structure makes it possible to combine fixed road-surface attributes, such as roughness, waviness, defect density, and grade, with passage-specific operational variables, including speed, payload state, braking events, suspension response, and fuel proxy. On this basis, the Road Condition Index (RCI), Dynamic Load Severity Index (DLSI), Fuel Penalty Factor (FPF), Braking Instability Indicator (BII), and Grade Severity Factor (GSF) are calculated.

The final stage of the framework is not interpreted as an uncontrolled causal experiment. Instead, the segment-level indicators are analyzed with explicit consideration of confounding factors, including longitudinal grade, payload state, truck model, mean speed, route identifier, and operating regime. This interpretation supports the identification of critical road segments and provides a reproducible basis for maintenance prioritization and predictive haul-road management.

2. Materials and Methods

The Materials and Methods section describes the field design and analytical procedures used in the present study. Literature references are retained only where they support the general methodological context; the main emphasis is placed on the field data acquisition campaign, preprocessing rules, synchronization procedure, indicator definitions, statistical models, and validation strategy. The analytical framework used in this study includes five consecutive components: field multisensor data acquisition, spatiotemporal alignment of heterogeneous records, construction of segment-level observations, calculation of derived road–vehicle–operation indicators, and confounder-aware statistical modelling with validation of segment rankings. This structure is used throughout the Methods section to distinguish the authors' analytical framework from a descriptive combination of sensor data and to separate road-surface degradation from geometric, resistance-related, and operational factors.

2.1. Study Site, Fleet, and Operating Conditions

The study was carried out on the intra-pit technological roads around the existing coal mine of the Ekibastuz deposit, operating in the conditions of intensive traffic of high-capacity mining dump trucks. The analyzed road network includes 12 main transport routes with a total length of 89.6 km, used for the transportation of rock mass between excavator-loading units and unloading points. Operating conditions are characterized by variable longitudinal grades in the range from 6.5 to 12.8%, curvilinear sections, local waviness zones, rutting areas, and zones of increased surface degradation. The upper part of this grade range exceeds the generally recommended level for safe and energy-efficient haul-road operation; therefore, segments with grades above 10% were treated in this study as engineering-constrained sections requiring particular attention in maintenance planning and possible profile correction.

In this study, three spatial and analytical terms are used consistently. A haul route denotes an operational truck movement path between loading and dumping or service zones. A monitored road segment denotes an engineering aggregation unit within the haul-road network; 12 monitored segments are labelled S1–S12. Segment boundaries were defined according to changes in grade, curvature, surface condition, local deterioration pattern, or traffic regime rather than by equal geometric length. A segment-level observation denotes one valid truck passage through one monitored segment after synchronization of

LiDAR-derived road attributes, GPS/IMU motion and vibration metrics, VIMS telemetry variables, and required covariates. Therefore, the statistical dataset consists of repeated segment-level observations nested within trucks, routes, and monitored road segments.

Caterpillar 785C and Caterpillar 785D mining dump trucks operated in loaded and empty modes were considered as transport units. For each class of equipment, five units of rolling stock were taken into account, and the total observation period was 6 weeks, which made it possible to cover 184 loaded and 176 empty passes along the analyzed segments. Field observations were carried out in the spring at typical temperatures between 5 and 18 °C and operational constraints typical of the region's open-pit coal mines, including dusting, local wetting of the pavement and high traffic of heavy equipment.

The choice of the object is due to the fact that the road network under consideration combines significant variability in the geometry of the route and high sensitivity of the transport process to the state of the road surface [21–23]. This makes it possible to quantify the relationship between the segmental degradation of the roadway, the dynamic response of the dump truck [24] and the energy and operational consequences in real production conditions [25,26].

Figure 2 presents a schematic layout of the analyzed open-pit haul-road network and defines the spatial units used for multisensor data aggregation. The scheme provides a structural representation of the monitored road network, including the loading zone, dumping zone, main haul-road direction, auxiliary/service branches, and the twelve analyzed road segments identified as S1–S12. These segment IDs are operational identifiers rather than equal-length geometric intervals. Each segment was defined according to the local road-engineering and operating context, including changes in grade, curvature, surface condition, or traffic regime. The figure introduces the field context of the Ekibastuz case and specifies the segment structure to which LiDAR-derived surface attributes, GPS/IMU trajectory and vibration records, and VIMS telemetry were assigned.



Figure 2. Schematic layout of the analyzed open-pit haul-road network and operational segment IDs used for multisensor data aggregation. The figure identifies the loading and dumping zones, principal haul-road direction, auxiliary/service branches, and segment IDs S1–S12 used to assign LiDAR-derived road-surface attributes, GPS/IMU trajectory and vibration records, and VIMS telemetry to common analytical units. The scheme is a structural representation of the monitored road network rather than a metric map.

Figure 2 functions as an engineering diagram rather than a cartographic route map. The 12 segment identifiers S1–S12 do not represent uniform intervals of fixed length; they represent road sections selected for segment-level analysis based on operational and engineering heterogeneity. The total length of the monitored road network was 89.6 km, while Figure 2 schematically shows its basic structural organization. Exact haulage distances, the direct distance from the pit to the waste dump, and the geometric proportions of the full mine road system are therefore defined by the underlying spatial dataset rather than by this schematic figure. Figure 2 defines the road segments used to assign LiDAR-derived surface attributes, GPS/IMU trajectory and vibration records, and VIMS telemetry to common spatial units. Segment boundaries are interpreted as engineering aggregation units associated with changes in grade, curvature, surface condition, and operating regime. This structure provides the spatial basis for calculating road-condition, dynamic-response, and operational-penalty indicators at the segment level.

Summary characteristics of the study site and transport fleet are given in Table 1.

Table 1. Study site and fleet characteristics.

Parameter	Value/Description
Study site	Operating open-pit coal mine of the Ekibastuz deposit
Active haul routes	12
Total haul-road length	89.6 km
Longitudinal slope range	6.5 to 12.8%
Road features	Curvature zones, waviness, rutting, degraded surface areas
Truck models	Caterpillar 785C; Caterpillar 785D
Trucks included in analysis	10
Observation period	6 weeks
Loaded passes	184
Empty passes	176
Season	Spring
Temperature range	5–18 °C

Table 1 specifies the field boundary conditions of the study, including the road-network scale, slope range, fleet composition, observation period, and number of loaded and empty passes.

2.2. Field Data Acquisition Campaign

In the present study, field data collection was organized as a multi-channel observation campaign combining remote laser scanning of the roadway, satellite-inertial monitoring of dump-truck movement, and onboard operational telemetry. The survey of the road surface was carried out in 8 UAV/LiDAR sorties with coverage of 96% of the studied road network. The total volume of spatial data was 1.24×10^9 cloud points, which ensured the restoration of the detailed three-dimensional geometry of the roadway.

After removing incomplete, anomalous, and unsynchronized records, the total observation array included 344 valid truck passes assigned to the 12 monitored road segments S1–S12. At the next stage, a final analytical dataset of 288 segment-level observations was formed and used for statistical analysis. Each observation corresponds to one valid truck passage through one monitored segment with complete LiDAR-derived road attributes, GPS/IMU motion and vibration metrics, VIMS telemetry variables, and required covariates. An additional reduction in the sample was caused by the exclusion of cases with incomplete LiDAR coverage, incomplete VIMS telemetry, or missing variables required for calculating the derived indicators and regression models used in this study.

Such a structure of the field campaign made it possible to provide a reproducible comparison of the geometric characteristics of the road surface, driving modes and machine

response in a single spatiotemporal contour. Thus, an empirical basis was formed for the subsequent statistical analysis of fuel-related penalties, dynamic load response and instability of the transport cycle.

The structure of the field campaign and the composition of the final data array are presented in Table 2.

Table 2. Field campaign structure and dataset composition.

Data Source	Observation Unit	Sampling Rate	Raw Records	Filtered Records	Analytical Output
UAV/LiDAR	Flight strip/road scan	~200 points/m^2	8 flights	8 flights	3D road model, defect maps, profile lines
GPS	Truck trajectory	10 Hz	360 trips	344 trips	Position, speed, grade, segment timing
IMU	Inertial signal	100 Hz	360 trips	344 trips	Vertical acceleration, vibration metrics
VIMS	On-board telemetry	1 Hz	360 trips	344 trips	Suspension pressure, gear shifts, braking events, fuel proxy
Integrated dataset	Segment-level observation	—	360 trips	344 trips	288 synchronized segment-level observations across 12 monitored road segments

Table 2 summarizes the observation channels, sampling rates, raw records, filtered records, and analytical outputs used to construct the final dataset of 288 segment-level observations across the 12 monitored road segments S1–S12.

2.3. Instrumentation and Sensing Architecture

Spatial assessment of the roadway condition was carried out using the DJI Matrice 300 RTK unmanned aerial vehicle (UAV) platform equipped with the Zenmuse L1 light detection and ranging (LiDAR) sensor [27]. This system was used to build a three-dimensional model of the road surface to identify local deformations, undulation zones, ruts, potholes and areas with a violation of the design profile. The resulting spatial products used in this study included a digital roadway-surface model, profile lines, road-surface mesh, and defect maps.

The kinematic parameters of the movement of mining dump trucks were recorded by the Racelogic VBOX Micro GPS monitoring system, which provides recording of coordinates, speed, trajectory, longitudinal route profile and variations of the driving mode at the level of individual segments [28]. In the analytical dataset, these records were used to calculate segment speed, speed variability, braking-event density, and segment traversal time.

The dynamic and operational response of the machine was analyzed using data from inertial measurement unit (IMU) sensors and the Caterpillar Vital Information Management System (VIMS) onboard system. The analysis included vertical accelerations, suspension pressure variations, gearshift intensity, frequency of braking events, operational signs of units, and other indicators [29] sensitive to road deterioration. The combined use of these three observation channels made it possible to move from a disparate description of the surface and traffic to a quantitative assessment of operationally significant road damage [30]. The composition of the measurement architecture, the recorded parameters and their analytical role are given in Table 3.

In Table 3, qVIMS denotes the relative fuel-use signal obtained from the Caterpillar VIMS telemetry stream. In this study, it was used as a dimensionless operational proxy of segment-level fuel burden rather than as a direct high-precision fuel-flow measurement in L/h or L/km. The value reflects the relative fuel-related load recorded by the onboard monitoring system during a truck pass and is therefore suitable for comparing segments under similar operating conditions. Because the signal may also be affected by payload

state, grade, speed regime, truck model [31], engine condition, and operator behavior, it was interpreted as a fuel proxy and not as an isolated measure of actual fuel consumption.

Table 3. Instrumentation, recorded variables, and analytical roles.

System/Device	Recorded Variable	Unit	Sampling Rate	Derived Feature	Analytical Role
DJI Matrice 300 RTK + Zenmuse L1	3D point cloud, surface geometry	points, m	~200 points/m^2	Roughness, waviness, defect density, rutting, grade	Road morphology and defect mapping
Racelogic VBOX Micro	Position, speed, trajectory	m, m/s	10 Hz	Segment speed, speed variance, travel time	Kinematics and travel stability
IMU sensors	Vertical acceleration, angular response	m/s^2, °/s	100 Hz	RMS acceleration, vibration intensity	Dynamic load response
Caterpillar VIMS	Suspension pressure, gear position, braking/acceleration events, relative fuel-use signal qVIMS	kPa, count, dimension-less	1 Hz	Pressure range, gear-shift rate, braking-event density, segment-mean qVIMS	Operational response and fuel-related burden; proxy-based, not direct fuel-flow measurement

The VIMS-derived variable qVIMS was not independently calibrated against fuel-flow meters, tank-level measurements, refuelling logs, or engine-bench measurements for the full field dataset. Therefore, it is not converted into L/h, kg/h, or L/km in this study. The variable is used only as a relative diagnostic proxy for segment-level comparison under comparable payload, truck-class, route-context, and operating-regime conditions. Consequently, all fuel-related results are reported as proxy-based relative burden rather than as absolute fuel-consumption, fuel-cost, or fuel-saving estimates.

2.4. Data Preprocessing, Synchronization, and Quality Control

Data preprocessing was performed separately for each sensor loop. For LiDAR point clouds, noise removal, georeferencing, filtering of non-surface objects, and roadway selection operations were used. On the basis of the cleaned cloud, digital surface profiles were formed and morphometric features were calculated, including roughness, waviness, density of local defects, and longitudinal profile characteristics [32].

GPS data were cleaned of anomalous coordinate outliers, interpolated short-term gaps, aligned timestamps and transformed trajectories into a single spatial coordinate system. For IMU and VIMS signals, high-frequency interference filtering, transient artifact removal, timeline normalization, and GPS synchronization were performed [33,34]. The synchronization procedure was performed in three stages. First, all telemetry streams were converted to a common timestamp format, and GPS time was used as the reference temporal axis. Second, truck trajectories were map-matched to the haul-road polyline and assigned to predefined road segments using chainage coordinates. Third, IMU and VIMS signals were aggregated within the time interval during which a given truck passed a given road segment. High-frequency IMU signals were summarized by RMS acceleration, peak acceleration, and vibration-intensity metrics, whereas lower-frequency VIMS records were aggregated as pressure range, gear-shift density, braking-event density, and fuel-proxy statistics. LiDAR-derived surface features were treated as spatially fixed segment attributes and linked to each segment by its start and end chainage. Observations were excluded if trajectory continuity, LiDAR coverage, VIMS completeness, or timestamp consistency did not satisfy the quality-control criteria. This procedure produced a segment-level dataset in which each observation corresponds to one truck passage through one road segment.

Because the input data streams differed in physical meaning, spatial resolution, temporal resolution, and sampling frequency, the synchronization procedure was organized at the segment level rather than as a direct point-to-point merging of raw records. GPS

trajectories were used as the primary spatiotemporal reference because they provided both timestamped truck positions and route progression along the haul road. LiDAR data were treated as spatially fixed road-surface attributes, whereas IMU and VIMS records were treated as passage-specific dynamic and operational responses. The alignment rules used to convert these heterogeneous records into a common segment-level observation structure are summarized in Table 4.

Table 4. Data alignment rules used for multisensor segment-level synchronization.

Data Source	Native Data Form	Alignment Reference	Segment-Level Aggregation	Quality-Control Criterion
LiDAR	Georeferenced point cloud/surface mesh	Road chainage and segment polygon	Roughness, waviness, defect density, rutting, grade	Sufficient surface coverage; removal of non-road objects and scanning artefacts
GPS	Timestamped position and speed	GPS time and route chainage	Segment entry and exit time, mean speed, speed variability, travel time	Trajectory continuity; realistic speed values; reliable segment boundary crossing
IMU	High-frequency inertial signal	GPS-derived truck-pass interval	RMS acceleration, peak acceleration, vibration-intensity metrics	Valid inertial signal over the segment pass interval; removal of transient artefacts
VIMS	Onboard telemetry records	GPS-derived truck-pass interval	Suspension-pressure range, braking-event density, gear-shift density, fuel proxy	Telemetry completeness; timestamp consistency with GPS and IMU records
Integrated observation	One truck pass through one road segment	Segment ID and truck-pass interval	Common feature vector for indicator calculation and statistical modelling	Exclusion of incomplete, unsynchronized, or inconsistent records

Table 4 clarifies that the final analytical dataset was not formed by forcing all sensors to the same sampling rate. Instead, each data source was transformed into features appropriate to its native resolution and then linked to the same road segment and truck-pass interval. This approach preserves the spatial detail of LiDAR-derived road morphology, the temporal structure of GPS-based truck movement, the high-frequency information of IMU response, and the operational content of VIMS telemetry. As a result, each observation used in the statistical analysis corresponds to one truck passage through one road segment and contains a consistent set of road-surface, kinematic, dynamic-response, and operational variables.

Variable normalization was performed after synchronization and quality control, but before indicator calculation and regression modelling. Two normalization procedures were used for different analytical purposes. For the calculation of composite indicators, including RCI and DLSI, min–max normalization was applied to transform each component variable into the interval [0,1]. The direction of each variable was checked before normalization so that higher normalized values consistently corresponded to more severe road condition, stronger dynamic response, or greater operational burden. For regression modelling, continuous predictors were additionally standardized using z-score normalization to improve numerical comparability of coefficients and reduce scaling effects. Categorical variables, including truck model, payload state, and route identifier, were encoded as dummy variables. Descriptive tables retained the original engineering units. Table 5 summarizes the normalization rules used for the main variable groups.

Table 5. Variable normalization rules used before indicator calculation and statistical modelling.

Variable Group	Examples	Normalization Used for Composite Indicators	Scaling Used for Regression Models	Direction Handling
Road-surface variables	Roughness, waviness, rutting, defect density	Min–max normalization to [0,1]	z-score standardization	Higher value = more severe surface degradation
Geometric and resistance variables	Mean grade, maximum grade, rolling resistance, curvature radius	Min–max normalization where used in GSF/RCI	z-score standardization	Grade and rolling resistance: higher = more severe; curvature radius was direction-adjusted so smaller radius corresponds to higher severity
Dynamic-response variables	RMS vertical acceleration, peak acceleration, suspension-pressure variability	Min–max normalization to [0,1]	z-score standardization	Higher value = stronger dynamic response
Operational variables	Braking density, gear-shift rate, travel time, fuel proxy	Min–max normalization where included in derived indicators	z-score standardization	Higher value = greater operational burden
Categorical variables	Payload state, truck model, route identifier	Not used in min–max composite scaling	Dummy-variable encoding	Reference category specified in model setup
Descriptive variables	Segment length, number of passes, temperature range	Not normalized	Retained in original units unless used as predictors	Interpreted in original engineering units

As shown in Table 5, min–max normalization was used only for constructing dimensionless composite indicators, whereas z-score standardization was used for regression predictors. This separation was introduced to preserve the interpretability of RCI, DLSI, FPF, BII, and GSF while allowing regression coefficients to be compared across variables measured in different units.

Because the data sources differed substantially in temporal and spatial resolution, synchronization was not performed as direct point-to-point merging of raw records. GPS trajectories were used as the primary spatiotemporal reference because they contained both timestamped position and route progression. Each truck trajectory was projected onto the haul-road centerline, and a chainage coordinate was calculated for each GPS point. Segment entry and exit times were then determined from the intersection of the trajectory with the predefined segment boundaries. LiDAR-derived variables were treated as spatial segment attributes and were calculated within the corresponding segment polygon or chainage interval. IMU and VIMS records were assigned to the same segment by selecting all observations recorded between the GPS-derived entry and exit times of the truck pass. High-frequency IMU signals were aggregated into RMS, peak, and variability metrics, whereas lower-frequency VIMS signals were summarized as pressure range, braking-event density, gear-shift density, and fuel-proxy statistics. Thus, the final dataset did not require equal sampling frequencies across sensors; instead, all signals were transformed into a common segment-level observation structure.

Uncertainty was considered at three levels. First, measurement-level uncertainty was reduced through coordinate cleaning, georeferencing, trajectory-continuity checks, and removal of incomplete telemetry records. Second, aggregation-level uncertainty was reduced by using segment-level summary metrics rather than individual raw samples, which limits the influence of local timestamp mismatch and short-term signal noise. Third, model-level uncertainty was assessed through confidence intervals of regression coefficients, bootstrap resampling, repeated subsampling, and leave-one-route-out validation. The stability of segment classification was additionally evaluated using repeated passes and repeatability-

oriented statistics, including the intraclass correlation coefficient, coefficient of variation, and Kendall's W. Therefore, the reported segment rankings should be interpreted as robust field-supported estimates rather than as exact deterministic values.

Quality control was applied before indicator calculation. Observations were excluded when one of the following conditions occurred: discontinuity of the GPS trajectory within a segment, unrealistic speed values, absence of a reliable segment entry or exit time, insufficient LiDAR coverage of the segment surface, incomplete VIMS telemetry over the truck-pass interval, or timestamp inconsistency between GPS, IMU, and VIMS records. Short internal gaps in GPS or telemetry records were accepted only when they did not affect the identification of segment boundaries or the calculation of aggregated metrics. Records with incomplete sensor coverage were not imputed for the main analysis, because artificial reconstruction of missing road-response signals could bias DLSI, FPF, and BII estimates. After these checks, 4.4% of records were excluded, and the quality-controlled dataset was used for subsequent indicator calculation and statistical modelling. Such a pipeline provided a reproducible basis for the subsequent calculation of derived indicators and statistical modelling.

Figure 3 presents the preprocessing, synchronization, and quality-control workflow used to transform heterogeneous field measurements into a unified segment-level analytical dataset. The scheme clarifies the sequential transition from independent LiDAR, GPS, IMU, and VIMS records to quality-controlled observations assigned to specific haul-road segments. The figure is presented as a technical workflow diagram in which each block corresponds to a reproducible data-processing operation.

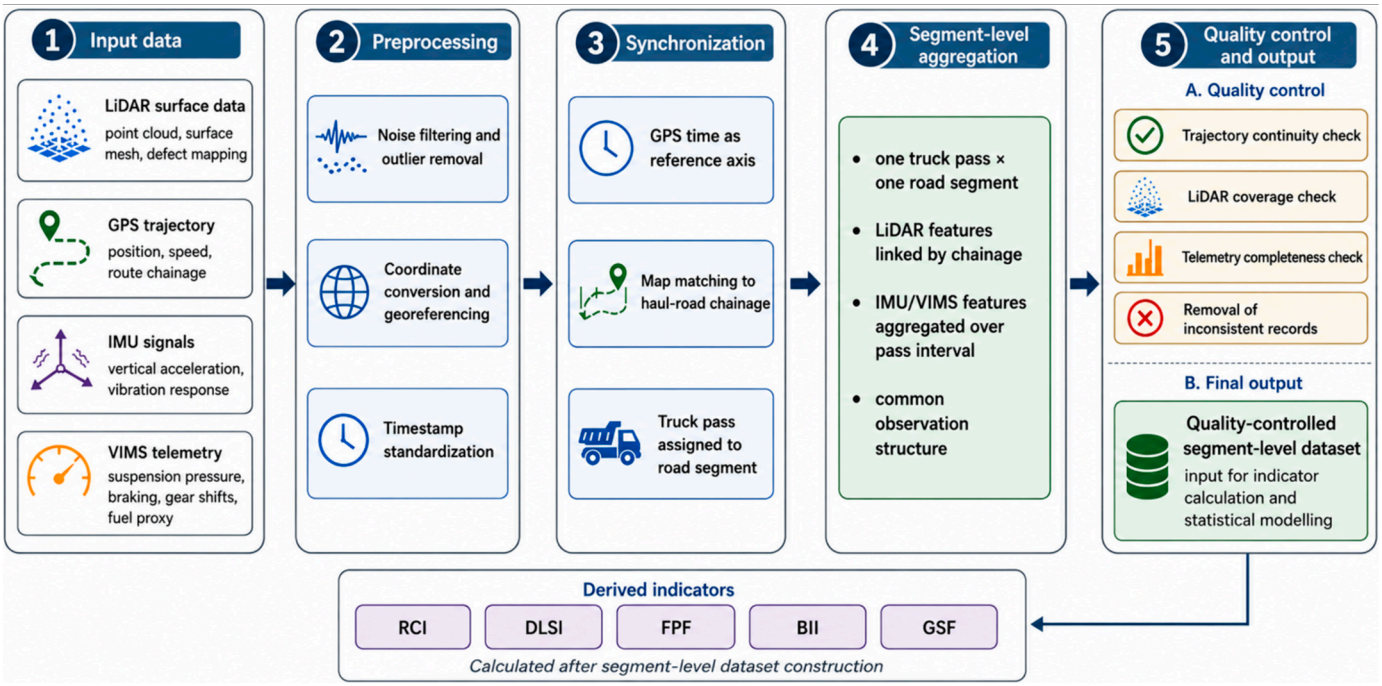


Figure 3. Preprocessing, synchronization, and quality-control workflow for multisensor field data.

Figure 3 shows that the multisensor dataset was formed through a sequential procedure rather than by direct merging of independent records. At the preprocessing stage, LiDAR data were filtered and georeferenced, GPS trajectories were converted to a common spatial reference, and IMU/VIMS records were standardized by time. At the synchronization stage, GPS time was used as the temporal reference axis, while haul-road chainage was used as the spatial reference for assigning truck passes to road segments.

The resulting segment-level observation corresponds to one truck pass through one road segment. This structure allows LiDAR-derived road-surface features to be linked with passage-specific IMU and VIMS variables, including vertical acceleration, suspension-pressure variability, braking events, gear shifts, and fuel proxy. Quality-control procedures were then applied to remove records with trajectory discontinuities, insufficient LiDAR coverage, incomplete telemetry, or inconsistent timestamps. The final quality-controlled dataset served as the basis for calculating RCI, DLSI, FPF, BII, and GSF indicators and for subsequent statistical modelling.

2.5. Segment Definition and Feature Extraction

The basic unit of analysis in this study is an operationally defined road segment rather than a fixed-length interval. Segment boundaries were selected according to changes in longitudinal grade, curvature, surface condition, local deterioration pattern, and traffic or operating regime. This segmentation allows road geometry, motion parameters, and machine response to be compared within road sections with internally consistent engineering conditions [35].

For each segment, a vector of spatial, kinematic, and operational features was calculated. Spatial features included surface roughness metric, surface waviness metric, local defect density, average and maximum longitudinal slope, and route curvature indicators. Kinematic features included mean velocity, velocity variance, density of braking events, and segmental transit time [36]. Performance features included RMS vertical acceleration, suspension pressure range, gearshift frequency, and fuel load or proxy views.

Thus, each segment was described by a feature vector of the form

$$\mathbf{x}_{seg} = [x_1, x_2, \ldots, x_n],$$

where the vector components reflected both the condition of the road surface and the response of the mining truck to the passage of this section. This form of representation made it possible to move from the analysis of individual signals to a holistic segment-level model of road-vehicle interaction. Table 6 presents a system of segment features, their dimensions, sources and aggregation rules.

Table 6. Segment-level variables, units, and aggregation rules.

Variable	Unit	Source	Aggregation	Interpretation
Surface roughness metric	—	LiDAR	mean	Micro-irregularity severity
Surface waviness metric	—	LiDAR	mean/max	Macro-profile instability
Defect density	defects/km	LiDAR	density	Local damage concentration
Mean longitudinal grade	%	LiDAR + GPS	mean	Average slope burden
Maximum longitudinal grade	%	LiDAR + GPS	max	Extreme profile burden
Segment speed	km/h	GPS	mean	Motion regime
Speed variance	$(km/h)^2$	GPS	variance	Flow instability
Braking density	events/km	GPS + VIMS	density	Regime instability
Segment travel time	s	GPS	mean	Traversal efficiency
RMS vertical acceleration	m/s^2	IMU	mean/max	Dynamic excitation
Suspension pressure range	kPa	VIMS	range	Load variability
Gear-shift rate	shifts/km	VIMS	density	Powertrain instability
Fuel proxy	relative	VIMS	mean	Energy burden

Table 6 defines the segment-level feature matrix used in the subsequent indicator calculation [37] and regression analysis.

Figure 4 shows the characteristic longitudinal profiles and morphological patterns for the good, moderate, and critical class segments.

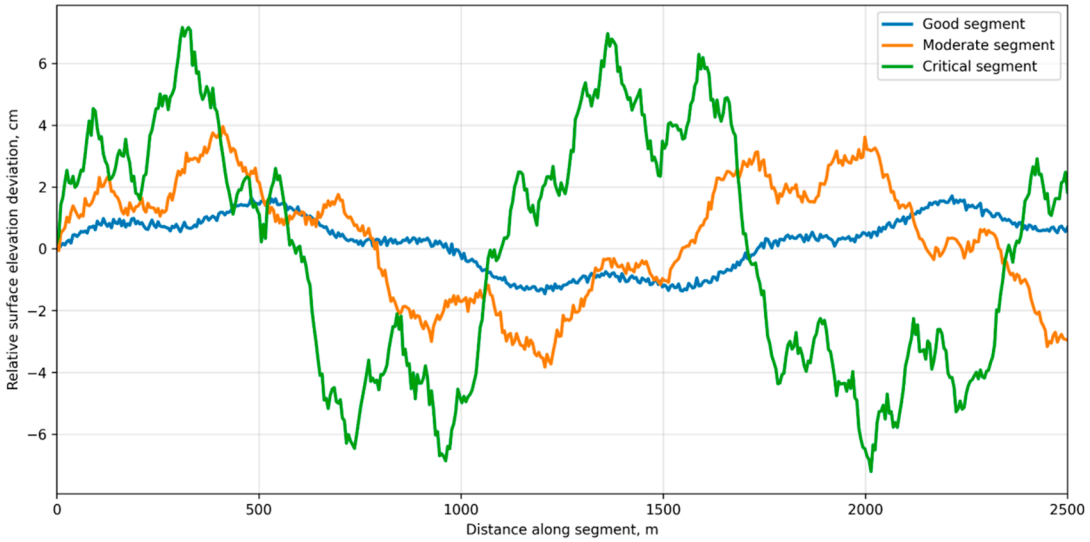


Figure 4. Representative surface profiles for good, moderate, and critical segments.

Figure 4 illustrates the increasing amplitude and spatial persistence of surface-profile deviations across the good [38], moderate, and critical segment classes.

2.6. Derived Indicators for Road Condition, Dynamic Response, and Operational Penalty

Before calculating the composite indicators, all continuous component variables were transformed into dimensionless values using min–max normalization:

$$x_{s,i} = \frac{x_i - \min(x_i)}{\max(x_i) - \min(x_i)}$$

where $x_{s,i}$ is the original value of component i for segment s; $x_{s,i}$ is the normalized value; and $\min(x_i)$ and $\max(x_i)$ are calculated within the quality-controlled field dataset. For variables where lower original values indicate higher severity, such as curvature radius, the direction was reversed before normalization. Thus, higher normalized values consistently indicate more severe surface degradation, stronger mechanical dynamic response, greater grade burden, or higher operational instability.

For regression modelling, continuous predictors were additionally standardized using z-score scaling. This separation was introduced because min–max normalization preserves the engineering interpretability of composite indices, whereas z-score scaling improves comparability of regression coefficients across variables measured in different units.

To move from an array of heterogeneous measurements to a single system of quantitative interpretation, derived indicators of road condition, dynamic response and operational damage were used in the work. The Road Condition Index (RCI) was revised as a surface-condition index only. It includes surface roughness, surface waviness, rutting or wheel-path deformation, and local defect density. Longitudinal grade and grade-related profile burden are not included in RCI in the revised formulation because they are represented separately by the Grade Severity Factor (GSF) and by grade-related covariates in the regression models. This separation avoids double-counting of grade-related effects and allows surface degradation to be interpreted separately from geometric burden.

$$RCI_s = \sum_{i=1}^{m} w_i x_{s,i}^{\text{surf}}$$

where RCI_s is the road-condition index for segment s; $x_{s,i}^{\text{surf}}$ is the normalized surface-condition component; wiw_iwi is the corresponding dimensionless weight; and mmm is the number of surface-condition components.

All components were normalized to the interval [0,1], and the weights were constrained as $\sum_{i=1}^{m} w_i = 1$.

The Dynamic Load Severity Index (DLSI) was used to describe the truck dynamic response within the same segment:

$$DLSI_s = \alpha_1 \tilde{a}_{\text{RMS},s} + \alpha_2 \Delta p_{\text{susp},s} + \alpha_3 \tilde{n}_{\text{brake},s} + \alpha_4 \tilde{n}_{\text{shift},s},$$

where $DLSI_s$ is the Dynamic Load Severity Index for segment s; $\tilde{a}_{\text{RMS},s}$ is the normalized RMS vertical acceleration; $\Delta p_{\text{susp},s}$ is the normalized suspension-pressure range; $\tilde{n}_{\text{brake},s}$ is the normalized braking-event density; $\tilde{n}_{\text{shift},s}$ is the normalized gear-shift density; and α_1, α_2, α_3, α_4 are weighting coefficients. These coefficients are dimensionless and sum to 1. They were assigned according to the expert-informed engineering weighting scheme described below.

The Fuel Penalty Factor (FPF) was used to characterize the relative fuel-related burden of a road segment:

$$FPF_s = \frac{q_{\text{seg},s} - q_{\text{ref}}}{q_{\text{ref}}},$$

where FPF_s is the fuel-penalty factor for segment s; $q_{\text{seg},s}$ is the segment-mean VIMS-derived relative fuel-use signal for segment s; and q_{ref} is the reference fuel-proxy value obtained for a low-severity segment or reference operating condition with comparable truck class and payload state. Both $q_{\text{seg},s}$ and q_{ref} are dimensionless proxy values; therefore, FPF_s is interpreted as a relative fuel-burden indicator rather than as a direct fuel-flow measurement.

The Braking Instability Indicator (BII) was calculated as a normalized combination of braking-event density and speed variability:

$$BII_s = \lambda_1 \tilde{n}_{\text{brake},s} + \lambda_2 \tilde{\sigma}_{v,s},$$

where BII_s is the braking-instability indicator for segment s; $\tilde{n}_{\text{brake},s}$ is the normalized braking-event density; $\tilde{\sigma}_{v,s}$ is the normalized speed variability within the segment; and λ_1 and λ_2 are dimensionless weighting coefficients satisfying $\lambda_1 + \lambda_2 = 1$.

The Grade Severity Factor (GSF) was used to describe the longitudinal-profile burden:

$$GSF_s = \gamma_1 \tilde{g}_{\text{mean},s} + \gamma_2 \tilde{g}_{\text{max},s},$$

where GSF_s is the grade-severity factor for segment s; $\tilde{g}_{\text{mean},s}$ is the normalized mean longitudinal grade; $\tilde{g}_{\text{max},s}$ is the normalized maximum longitudinal grade; and γ_1 and γ_2 are dimensionless weighting coefficients satisfying $\gamma_1 + \gamma_2 = 1$.

Thus, the coefficients w_i, α_i, λ_i, and γ_i denote dimensionless weights used to aggregate normalized variables into composite indicators. They do not represent fitted regression parameters. Their role is to define the relative engineering importance of each component within the corresponding indicator.

The Dynamic Load Severity Index (DLSI) was revised as a mechanical dynamic-response indicator. It includes RMS vertical acceleration, peak vertical acceleration, suspension-pressure variability, and vibration-intensity metrics. Braking-event density and gear-shift rate were excluded from DLSI because they may partly reflect driver behavior, route context, payload state, speed regulation, and operating regime. These variables are

treated separately as operational-response covariates and are partly represented in the Braking Instability Indicator (BII).

$$DLSI_s = \lambda_1 a_s^{\mathrm{RMS}} + \lambda_2 a_s^{\mathrm{peak}} + \lambda_3 p_s^{\mathrm{susp}} + \lambda_4 vib_s$$

where $DLSI_s$ is the Dynamic Load Severity Index for segment s; a_s^{RMS} is normalized RMS vertical acceleration; a_s^{peak} is normalized peak vertical acceleration; p_s^{susp} is normalized suspension-pressure variability; vib_s is the normalized vibration-intensity metric; and $\lambda_1 - \lambda_4$ are dimensionless weights constrained to sum to unity. The baseline weights used for RCI and DLSI are summarized in Table 7.

Table 7. Baseline weighting coefficients used for RCI and DLSI calculation.

Indicator	Component	Weight	Rationale
RCI	Surface roughness	0.35	Direct indicator of micro-irregularity severity and wearing-course condition
RCI	Surface waviness	0.30	Descriptor of macro-profile instability and repeated vertical excitation
RCI	Rutting/wheel-path deformation	0.20	Reflects traffic-induced wheel-path deformation
RCI	Local defect density	0.15	Represents localized damage concentration
DLSI	RMS vertical acceleration	0.35	Primary indicator of sustained vertical dynamic excitation
DLSI	Peak vertical acceleration	0.30	Captures short-duration high-severity dynamic events
DLSI	Suspension-pressure variability	0.25	Represents load transfer and suspension response
DLSI	Vibration-intensity metric	0.15	Characterizes persistent vibration exposure during segment traversal

As shown in Table 7, the adopted weighting scheme gives priority to physically interpretable road and vehicle-response variables, but does not exclude secondary operational indicators. The weights should therefore be interpreted as expert-informed engineering coefficients rather than statistically optimized parameters. To evaluate whether the resulting segment ranking depends strongly on the selected coefficients, a sensitivity analysis of alternative weighting schemes was performed in Section 3.6.

The relative fuel-related operational burden of a road segment was characterized by the Fuel-Use Proxy Burden Factor (FPF), defined as the relative excess of the VIMS-derived fuel-use proxy compared with a reference segment or reference operating condition:

$$FPF_s = \frac{q_{seg,s} - q_{ref}}{q_{ref}},$$

where $q_{seg,s}$ is the segment-mean VIMS-derived fuel-use proxy for segment sss, and q_{ref} is the corresponding reference proxy value obtained for a low-severity segment or comparable reference operating condition. Both $q_{seg,s}$ and q_{ref} are dimensionless proxy values. Therefore, FPF_s is interpreted as a relative proxy-based fuel-burden indicator and not as a direct measurement of absolute fuel consumption.

In addition, the Braking Instability Indicator (BII) was used to assess the instability of the driving mode, which reflects the frequency and recurrence of braking events in combination with speed variations, and the severity of the longitudinal profile was characterized by the *GSF* indicator, which takes into account the average and extreme slopes of the segment.

Such a system of indicators made it possible to move from the description of individual road defects to the quantitative assessment of their operational significance [39], which is especially important for the subsequent ranking of sections by the degree of operational criticality and the priority of repair impacts.

All symbols used in the derived-indicator formulas are defined at their first occurrence. The following notation convention is adopted to ensure reproducibility and clarity of the indicator calculations without reliance on implicit or undefined parameters:

Subscript s denotes the analyzed road segment;

The tilde symbol denotes a normalized variable (scaled to the interval [0,1]);

q denotes the VIMS-derived fuel-use proxy signal;
n denotes event density (e.g., braking or gear-shift events per unit distance or time);
σv denotes speed variability within a segment;
g denotes longitudinal grade (slope);
w_i, α_i, λ_i, and γ_i denote dimensionless weighting coefficients, each set constrained to sum to unity: $\sum_{i=1}^{m} w_i = 1$, $\sum_{j=1}^{4} \alpha_j = 1$, $\lambda_1 + \lambda_2 = 1$, $\gamma_1 + \gamma_2 = 1$.

This notation was introduced to ensure that the indicator calculations can be reproduced without relying on implicit or undefined parameters. Table 8 summarizes the formulas, physical meaning and practical role of derived indicators.

Table 8. Derived indicators, formulas, physical meaning, and practical use.

Indicator	Formula/Basis	Physical Meaning	Practical Use
Road Condition Index (RCI)	Weighted normalized road-condition metrics	Integral road-condition quality	Ranking of degraded segments
Dynamic Load Severity Index (DLSI)	Weighted normalized dynamic-response metrics	Dynamic stress imposed on the truck	Maintenance prioritization
Fuel-Use Proxy Burden Factor (FPF)	$\frac{q_{seg} - q_{ref}}{q_{ref}}$	Relative VIMS-derived fuel-use proxy burden	Comparative segment-level diagnosis of fuel-related operating burden
Braking Instability Indicator (BII)	Braking density + speed variability	Motion instability	Safety and drivability analysis
Grade Severity Factor (GSF)	Mean and extreme grade metrics	Severity of longitudinal profile	Route correction and design optimization

Table 8 summarizes the derived indicators used to describe road condition, truck dynamic response, fuel-related penalty, braking instability, and grade severity. The full names of all derived indicators are provided in the table at their first tabular occurrence; the corresponding abbreviations are used consistently in the subsequent analysis. These indicators [40] are not interpreted as proof of a single causal pathway from surface degradation to fuel use. Instead, they provide a structured segment-level description that allows road-surface condition, longitudinal profile, rolling resistance, vehicle response, and operational penalties to be analyzed jointly.

2.7. Treatment of Confounding Factors and Interpretation of Effects

Because fuel use, dynamic response, and travel time are affected by several interacting factors, the analysis was explicitly formulated as a controlled field association study rather than as a direct causal experiment. Road-surface degradation was therefore not interpreted in isolation. The statistical framework separated, as far as permitted by the available data, three groups of explanatory factors: surface-condition factors, including roughness, waviness, rutting, and defect density; geometric and resistance-related factors, including mean grade, maximum grade, rolling resistance, and curvature radius; and operational factors, including payload state, mean speed, truck model, route identifier, braking-event density, and operating regime.

This distinction is necessary because increased fuel use or dynamic response on a steep segment may be caused partly by longitudinal grade and rolling resistance rather than by poor surface condition alone. Conversely, a moderately sloped segment with high roughness, waviness, or defect density may still generate high vibration response and braking instability. For this reason, the statistical models used grade-related and

rolling-resistance variables as explicit covariates rather than treating them as part of the surface-degradation effect. Payload state, mean speed, truck model, and route identifier were also included where available to reduce operational confounding.

Not all potential confounders could be directly measured in the field campaign. Truck age, engine condition, tire pressure, tire wear, individual operator skill, altitude variations, and queueing time at loading and dumping points were not available as fully independent continuous variables for all observations. These factors are therefore acknowledged as residual confounders. To avoid overstating the interpretation, the terms "effect" and "impact" in this analysis refer to statistically supported field associations under observed operating conditions, not to isolated causal effects established by a controlled experiment. The analytical separation of the main factor groups is summarized in Table 9.

Table 9. Separation of road-surface, geometric, resistance-related, and operational factors in the segment-level analysis.

Factor Group	Variables Considered in the Study	Analytical Role	Interpretation
Road-surface degradation	Roughness, waviness, rutting, defect density, RCI	Main road-condition descriptors	Used to describe surface deterioration and its association with truck response and operational penalties
Longitudinal profile	Mean grade, maximum grade, GSF	Geometric control variables	Used to separate slope burden from surface-degradation effects
Rolling resistance and curvature	Rolling resistance, minimum curvature radius	Resistance-related and geometric covariates	Used to account for additional traction demand and speed constraints not caused only by surface defects
Vehicle and payload state	Truck model, payload state, mean speed	Operational control variables	Used to reduce confounding caused by vehicle class, loading condition, and driving regime
Driver and traffic regime	Braking-event density, route identifier, operating regime	Behavioural and route-context proxies	Used to partially account for route-specific and driving-pattern variability
Residual confounders	Truck age, engine condition, tire pressure, tire wear, operator skill, altitude, queueing at loading/dumping points	Unmeasured or partially observed factors	Acknowledged as limitations; results interpreted as associations rather than isolated causal effects

As shown in Table 9, the interpretation does not attribute fuel-related or dynamic-response variation to road-surface degradation alone. The segment-level models were used to examine whether surface-condition indicators remained associated with DLSI, FPF, BII, and travel-time variability after considering grade, rolling resistance, curvature, payload state, speed, truck model, and route context. This formulation improves methodological transparency and reduces the risk of confusing surface deterioration with geometric or operational burden.

2.8. Statistical Modelling Framework

Statistical processing of the data was aimed at quantifying the contribution of road degradation to the dynamic response of mining dump trucks [41], fuel and energy losses and traffic instability. At the first stage, a correlation analysis was carried out between the spatial characteristics of the road, machine response indicators and operational metrics [42]. This made it possible to preliminarily identify the most sensitive and informative signs.

At the second stage, four types of regression models were built. The first model described the dependence of the DLSI Dynamic Load Index on the geometric characteristics of the road segment:

$$DLSI_{seg} = \beta_0 + \beta_1 RCI_{seg} + \beta_2 GSF_{seg} + \beta 3 v_{seg} + \beta_4 S_{load} + \beta 5 C_{truck} + \varepsilon.$$

The second model was used to estimate the fuel surcharge:

$$FPF_{seg} = \gamma_0 + \gamma_1 RCI_{seg} + \gamma_2 DLSI_{seg} + \gamma_3 GSF_{seg} + \gamma_4 S_{load} + \gamma_5 C_{truck} + \eta.$$

The third model described the time it takes to pass a segment:

$$T_{seg} = \delta_0 + \delta_1 RCI_{seg} + \delta_2 BII_{seg} + \delta_3 GSF_{seg} + \delta_4 S_{load} + \delta_5 C_{truck} + \xi.$$

The fourth model was used to form an integral operational severity score designed for segmental prioritization of road repairs:

$$OPS_{seg} = \lambda_1 \widehat{RCI}_{seg} + \lambda_2 \widehat{DLSI}_{seg} + \lambda_3 \widehat{FPF}_{seg} + \lambda_4 \widehat{T}_{seg}.$$

Because the road–vehicle–operation system has a physically nested structure, an additional path-oriented interpretation was introduced. The purpose was not to claim a fully confirmatory causal SEM, because the study is observational, but to avoid interpreting RCI and DLSI as fully independent parallel predictors. The following cascade was considered:

$$RCI_s \rightarrow DLSI_{s,p} \rightarrow FPF_{s,p}.$$

with GSF, rolling resistance, curvature, payload state, speed regime, truck model, and route identifier treated as covariates.

The first equation describes the association between surface-condition severity and mechanical dynamic response:

$$DLSI_{s,p} = \alpha_0 + \alpha_1 RCI_s + \alpha_2 GSF_s + \alpha_3 RR_s + \alpha_4 Curv_s + \alpha_c C_{s,p} + \\ + u_{truck} + u_{segment} + u_{route} + \varepsilon_{s,p}$$

The second equation describes the association between VIMS-derived fuel-use proxy burden and both surface condition and dynamic response:

$$FPF_{s,p} = \beta_0 + \beta_1 RCI_s + \beta_2 DLSI_{s,p} + \beta_3 GSF_s + \\ + \beta_4 RR_s + \beta_c C_{s,p} + u_{truck} + u_{segment} + u_{route} + \varepsilon_{s,p},$$

where s denotes the monitored road segment; p denotes a truck pass; RR_s is rolling resistance; $Curv_s$ is curvature-related severity; $C_{s,p}$ is the vector of operational covariates; u_{truck}, $u_{segment}$, and u_{route} are grouped random terms or clustering terms; and $\varepsilon_{s,p}$ is the residual term.

In this path-oriented interpretation, β_1 represents the direct conditional association of surface condition with fuel-use proxy burden, while $\alpha_1\beta_2$ represents the indirect association through dynamic response. This formulation reflects the engineering pathway from road morphology to vehicle response and then to operational proxy burden.

To clearly illustrate the logic of the statistical interpretation, Figure 5 presents a path-oriented scheme in which road condition is treated as a surface descriptor, dynamic response as a mechanistic intermediate path, and fuel load as a relative proxy derived from VIMS data. The scheme also shows that slope, rolling resistance, curvature, load condition,

speed mode, truck type, and route context are considered as covariates and potential confounding factors, rather than as isolated causal mechanisms.

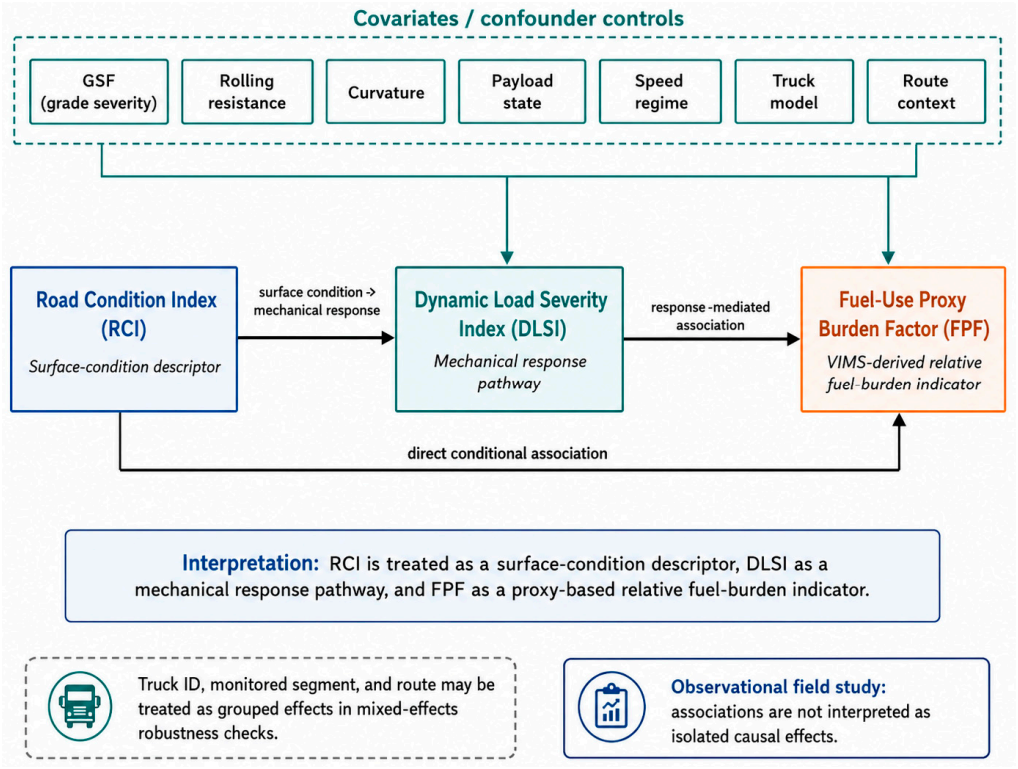


Figure 5. Path-oriented interpretation of the association between road-condition severity, mechanical dynamic response, and VIMS-derived fuel-use proxy burden. RCI is treated as a surface-condition descriptor, DLSI as a mechanical response pathway, and FPF as a proxy-based relative fuel-burden indicator. GSF, rolling resistance, curvature, payload state, speed regime, truck model, and route context are treated as covariates rather than as isolated causal mechanisms.

Figure 5 clarifies that the revised modelling framework is not interpreted as a direct cause-and-effect chain in a strict experimental sense. Instead, it represents a controlled field-based association structure in which road-condition severity may be linked to fuel-use proxy burden both directly and indirectly through the vehicle's mechanical dynamic response. This interpretation is methodologically important because it avoids treating RCI and DLSI as fully independent parallel causes and better reflects the physical logic of the haul-road–vehicle system under operational field conditions.

The parameters of the models were estimated by the robust linear regression method, and the quality of the fit was characterized by R^2, *RMSE*, *MAE* and confidence intervals of coefficients [43]. To exclude distortions associated with multicollinearity, variance inflation factor (VIF) analysis was carried out for all continuous predictors and dummy-variable groups. Model adequacy was additionally evaluated using residual diagnostics, including residual-versus-fitted plots, Q–Q plots, standardized residuals, Cook's distance, and tests for heteroscedasticity. The stability of the estimates was checked using bootstrap resampling, repeated subsampling, and leave-one-route-out validation [44].

The residual diagnostics are summarized in Table 10. The purpose of these diagnostics was not to claim laboratory-level causality, but to verify that the fitted regression models did not show strong multicollinearity, systematic residual structure, extreme influential observations, or severe heteroscedasticity that would invalidate the field-based associations.

Table 10. Multicollinearity and residual diagnostic summary for the regression models.

Diagnostic Criterion	Procedure Used	Summary Result	Interpretation
Multicollinearity	Variance inflation factor (VIF) analysis for continuous predictors and dummy-variable groups	All VIF values remained below the commonly used threshold of 5; most predictors were below 3	No severe multicollinearity was detected
Residual centering	Mean standardized residuals	Residual means were close to zero for all models	No systematic positive or negative bias was observed
Residual pattern	Residual-versus-fitted plots	No pronounced nonlinear residual structure was detected	Linear specification was acceptable for field-association modelling
Normality check	Q–Q plots of standardized residuals	Mild deviations were observed in the tails, but no dominant departure from approximate normality	Acceptable for robust regression and confidence-interval interpretation
Heteroscedasticity	Breusch–Pagan-type diagnostic and visual inspection	No severe heteroscedasticity was detected; robust standard errors were retained	Inference was treated conservatively
Influential observations	Cook's distance and standardized residual screening	No observation exceeded a critical influence level requiring exclusion	Segment rankings were not driven by a single observation
Ranking stability	Bootstrap, repeated subsampling, leave-one-route-out validation	Critical segments remained stable across resampling checks	Segment-priority results were robust to sample perturbation

As shown in Table 10, the regression models did not exhibit severe multicollinearity or diagnostic violations that would invalidate the reported field associations. The residual diagnostics indicated acceptable model behavior for the purpose of segment-level engineering interpretation. Nevertheless, because the study is observational and field-based, the regression results were interpreted as controlled associations rather than as isolated causal effects.

Because the field dataset contains repeated truck passes grouped by truck, monitored road segment, route context, and payload condition, the revised analysis additionally considered the hierarchical structure of the observations. Mixed-effects models with random intercepts were used as a robustness-oriented extension of the robust regression models:

$$Y_{s,p} = \beta_0 + \beta X_{s,p} + b_{truck} + b_{segment} + b_{route} + \varepsilon_{s,p},$$

where $Y_{s,p}$ denotes DLSI, FPF, BII, or segment travel time for pass p through segment s; $X_{s,p}$ is the vector of fixed predictors and covariates b_{truck}, $b_{segment}$, and b_{route} are random intercepts for truck ID, monitored segment, and route context; and $\varepsilon_{s,p}$ is the residual term. Payload state was treated as a fixed effect because it has direct physical meaning. Day, shift, and operator effects were not included as random effects because complete independent identifiers were not available for all observations; they are therefore acknowledged as residual confounders.

The structure of statistical models and the corresponding estimating metrics are provided in Table 11.

The predictor structure in Table 11 was designed to avoid attributing all operational variation to road-surface degradation. In particular, grade, rolling resistance, curvature

radius, payload state, speed, truck model, and route identifier were included as control variables or contextual covariates. Therefore, the regression coefficients were interpreted as conditional associations within the observed field dataset rather than as isolated causal effects.

Table 11. Statistical models, dependent variables, predictors, and evaluation metrics.

Model	Dependent Variable	Predictors/Covariates	Evaluation Metrics
A	DLSIseg	RCIseg, mean grade, maximum grade, rolling resistance, curvature radius, mean speed, payload state, truck model, route ID	R^2, root mean square error (RMSE), mean absolute error (MAE), and coefficient confidence interval (CI)
B	FPFseg	RCIseg, DLSIseg, mean grade, maximum grade, rolling resistance, curvature radius, payload state, truck model, route ID	R^2, *RMSE*, *MAE*, coefficient *CI*
C	Segment travel time (Tseg)	RCIseg, BIIseg, mean grade, maximum grade, rolling resistance, curvature radius, payload state, mean speed, truck model, route ID	R^2, *RMSE*, *MAE*, coefficient *CI*
D	Operational severity score (OPSseg)	Standardized RCI, DLSI, FPF, BII, GSF with bootstrap and leave-one-route-out rank stability	Rank stability, bootstrap consistency, Kendall's *W*
E	Path-oriented road–vehicle–proxy model	Stage 1: DLSI as a function of RCI and covariates; Stage 2: FPF as a function of RCI, DLSI, and covariates	Direct and indirect association signs, coefficient stability, bootstrap confidence intervals
F	Mixed-effects robustness model	DLSI, FPF, BII, or Tseg—Fixed effects: RCI, DLSI where appropriate, GSF, rolling resistance, curvature, payload state, mean speed, truck model; random intercepts: truck ID, monitored segment, route context	Marginal/conditional R^2, coefficient sign stability, rank stability

2.9. Validation Strategy and Uncertainty Assessment

Verification of the proposed approach was carried out at several levels. First, the consistency of the spatial anomalies of the road surface, identified by UAV/LiDAR data, with local peaks of dynamic response recorded by IMU and VIMS, was checked. The coincidence of geometrically defective segments with an increase in vertical acceleration, pressure variability in the suspension and the density of braking events was considered as a basic confirmation of the physical viability of the road–vehicle coupling scheme [45].

For this purpose, the values of RCI, *DLSI*, *FPF* and segment travel time (*Tseg)* obtained over independent passes were compared, and the stability of the segment classification was evaluated using the intraclass correlation coefficient (ICC), coefficient of variation (CV), and Kendall's coefficient of concordance (Kendall's W) coefficients before–after comparison. However, within the framework of this study, the main attention was focused on repeat-pass reproducibility, interloop consistency, and statistical stability of segment estimates [46].

Third, to assess the statistical stability of the model, bootstrap-resampling, repeated subsampling, and leave-one-route-out sensitivity analysis were used to check the stability of segment ranks and coefficient signs, which made it possible to determine the sensitivity of model coefficients and segment ratings to changes in sample composition [47]. This

multi-level approach made it possible to interpret the results not as a single observation, but as a reproducible diagnostic scheme for assessing operationally critical road segments.

Table 12 summarizes the basic verification procedures and the corresponding sustainability indicators.

Table 12. Validation procedures, robustness checks, and uncertainty metrics.

Validation Level	Procedure	Output
Spatial–dynamic consistency	LiDAR anomalies vs. IMU/VIMS peaks	Physical plausibility of road–vehicle coupling
Repeat-pass reproducibility	Repeated runs on same segment	ICC, CV, Kendall's (W)
Statistical robustness	Bootstrap, repeated subsampling	Stability of coefficients and rankings
Route sensitivity	Leave-one-route-out validation	Transferability across routes
Post-maintenance validation	Before–after monitoring after repair actions	Required for future verification of intervention effectiveness; not implemented in the present field campaign

Table 12 summarizes the verification procedures used to assess spatial–dynamic consistency, repeat-pass reproducibility [48], statistical robustness [49], and route sensitivity. The post-maintenance validation row is included as a required future verification stage, because repair interventions were not implemented and monitored within the present field campaign.

Figure 6 presents the verification algorithm used to assess the reliability of segment-level indicators and the stability of critical segment rankings. The framework links spatial anomalies obtained using LiDAR with truck-response measurements, repeatability of repeated passes, statistical robustness checks, and engineering interpretation. The figure is presented as a technical verification diagram, with each block corresponding to a specific verification procedure.

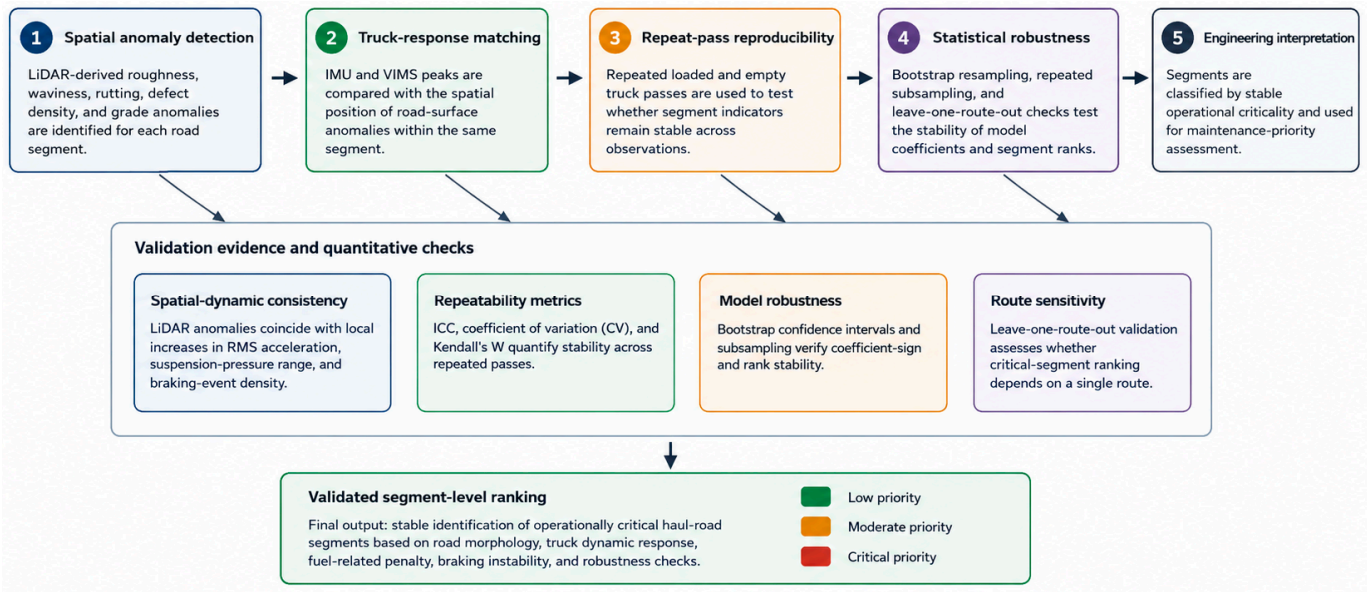


Figure 6. Validation workflow and repeatability assessment for segment-level indicators.

Figure 6 shows that validation was performed at several complementary levels. First, LiDAR-derived road-surface anomalies were compared with local increases in

truck dynamic response recorded by IMU and VIMS, including RMS vertical acceleration, suspension-pressure variability, and braking-event density. This step was used to verify the physical consistency of the road–vehicle coupling assumed in the segment-level framework. Second, repeated loaded and empty passes through the same road segments were used to assess the reproducibility of RCI, DLSI, FPF, BII, and GSF values. The stability of these indicators was evaluated using repeatability-oriented metrics, including the intraclass correlation coefficient, coefficient of variation, and Kendall's W. Third, bootstrap resampling, repeated subsampling, and leave-one-route-out validation were used to test the robustness of model coefficients and the stability of segment rankings. The final output of this procedure was a validated ranking of haul-road segments according to their operational criticality and maintenance priority [50].

2.10. Confounding Factors and Methodological Limitations

When interpreting the obtained dependencies, it was taken into account that the dynamic response of a mining dump truck is determined not only by the condition of the roadway, but also by a number of related factors [51]. Partially controllable factors included the weight of the transported cargo, the speed of movement, the mode of acceleration and braking, as well as the type of vehicle. Uncontrollable or limited controllable factors included the technical condition of the suspension and tires, local weather influences, surface moisture and variability in the driver's operational behavior [52].

An additional source of uncertainty was the integral nature of some VIMS indicators, which may reflect the combined effect of several factors. In addition, the accuracy of LiDAR reconstruction and GPS referencing could vary depending on the survey conditions and the complexity of the terrain. Nevertheless, the use of a multisensory scheme, segment aggregation, and quality-control procedures made it possible to minimize the influence of these factors and preserve the interpretability of the obtained relationships [53].

In this study, segment boundaries were not imposed as equal-length partitions. They were defined as operational road sections reflecting changes in longitudinal grade, curvature, surface condition, local deterioration pattern, or traffic regime. Thus, the segment IDs S1–S12 used throughout the manuscript are engineering aggregation units rather than constant-length geometric slices.

Consequently, these limitations do not negate the applicability of the proposed approach, but determine the framework for its correct use and indicate the directions for further expansion of the dataset, including through many seasonal observations, more detailed payload state accounting, and independent validation at other mining sites [54].

3. Results

3.1. Descriptive Statistics of the Field Dataset

Before analyzing the field-supported associations between roadway condition and operational response variables, a descriptive characteristic of the final analytical segment data array was performed. The final set included 288 valid segment observations selected from a total array of 344 cases after the stage of advanced feature completeness control and interloop synchronization. Of the 288 segment observations, 147 were loaded states and 141 were empty states. Critical segments accounted for 96 observations, moderate criticality segments accounted for 72 observations, and low-criticality segments accounted for 120 observations. This distribution ensured the comparability of morphological and operational effects between the classes of road conditions.

The RCI Road Condition Index ranged from 2.94 to 12.57, the *DLSI* Dynamic Load Index ranged from 2.10 to 13.31, and the *FPF* VIMS-derived fuel-use proxy burden factor ranged from 0.041 to 0.356. The average speed by segment was 26.0 km/h with a standard

deviation of 4.4 km/h, while longitudinal gradients reached 12.1% on the most difficult sections of the route.

Already at the level of descriptive statistics, it was clear that the segments of the road network differ significantly not only in terms of geometric characteristics, but also in terms of the operational response of the vehicle. This confirms the expediency of moving from route analysis as a whole to segment-level interpretation [55], in which road condition, vehicle response, and operational penalty are considered together.

To provide a transparent segment-level basis for the subsequent interpretation of road-condition indicators, dynamic-response metrics, and operational penalties, Table 13 summarizes the basic geometric, surface-condition, and operational characteristics of each analyzed haul-road segment. This table is introduced before the distribution analysis because the effects reported later in the Results section cannot be interpreted only as consequences of surface degradation; they must also be considered in relation to segment length, grade, rolling resistance, curvature, traffic regime, and the number of repeated truck passes.

Table 13. Basic geometric, surface-condition, and operational characteristics of the analyzed haul-road segments.

Segment	Length, km	Mean Grade, %	Max Grade, %	Rolling Resistance, %	Min. Curvature Radius, m	Defect Density, Defects/km	Waviness Index	Mean Speed, km/h	Loaded Passes, n	Empty Passes, n	Road-Condition Class
S1	6.8	2.1	3.4	2.4	420	0.8	0.21	31.8	12	11	Low
S2	7.1	3.4	5.2	3.1	310	1.6	0.38	29.4	13	12	Moderate
S3	6.5	4.0	6.1	3.4	280	1.9	0.42	28.7	12	12	Moderate
S4	7.4	6.8	9.7	5.2	190	4.8	0.76	23.6	13	12	Critical
S5	8.2	8.6	12.1	6.4	165	5.2	0.84	21.9	12	12	Critical
S6	6.9	5.1	7.2	4.0	145	2.1	0.47	27.3	12	11	Moderate
S7	7.8	7.4	10.6	5.8	205	4.3	0.88	22.7	13	12	Critical
S8	8.0	8.1	12.8	6.1	175	4.9	0.92	21.4	12	12	Critical
S9	7.3	3.0	4.8	2.9	360	1.1	0.29	30.2	12	12	Low
S10	7.6	3.7	5.6	3.2	335	1.3	0.33	29.1	12	12	Low
S11	8.1	2.4	3.9	2.5	460	0.7	0.18	32.4	12	11	Low
S12	7.9	2.0	3.5	2.3	510	0.6	0.16	33.0	12	12	Low

As shown in Table 13, the analyzed haul-road network is heterogeneous not only in terms of road-surface degradation, but also in terms of geometric and operational conditions. The critical segments S4, S5, S7, and S8 combine higher mean and maximum grades, increased rolling resistance, smaller curvature radii, higher defect density, and higher waviness values. This confirms that the subsequent variation in DLSI, FPF, BII, and travel-time indicators should not be attributed to surface degradation alone. Instead, the interpretation must consider the combined influence of surface condition, longitudinal profile, curvature-related constraints, and truck operating regime. Table 13 therefore provides the descriptive basis for the confounder-aware analysis and improves the repeatability of the segment-level results.

After defining the segment-level field context in Table 13, Figure 7 shows the distribution of key road, dynamic, and operational variables in the final segment observation array.

Figure 7 shows that the variability of parameters is not random and is not limited to one type of feature. The largest variation is observed simultaneously in the integral index of road condition, dynamic load and fuel surcharge, which indicates the presence of a pronounced heterogeneity of the road environment expands synchronously: segments with degraded coverage morphology, as a rule, show a wider spread of machine response. Thus, already at the level of primary data distribution, the general structure of road-related operational severity can be traced [56].

Summary descriptive characteristics of segment variables are given in Table 14.

Table 14 is important for further interpretation of the results, as it allows for quantification of the scale of heterogeneity of the system under study. It shows that the differences between the segments manifest themselves simultaneously in the morphology of the road

surface, the kinematics of traffic and operational losses. In particular, the almost four-fold range of change in FPF and more than a six-fold spread in braking density indicate that road degradation within the same network forms qualitatively different conditions for the route [57]. This is what makes segment-level analysis methodologically sound and practically relevant.

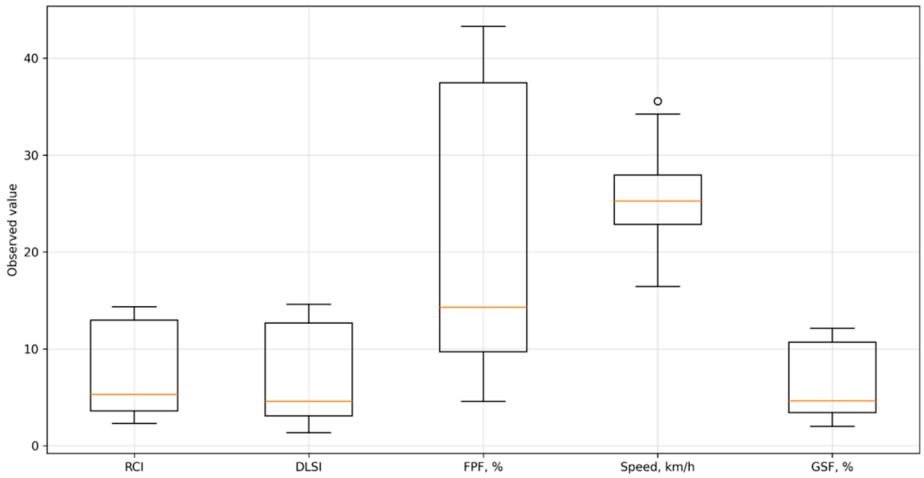


Figure 7. Distribution of key road, vehicle, and operational variables in the field dataset.

Table 14. Descriptive statistics of segment-level variables.

Variable	Min	Max	Mean	SD
RCI	2.94	12.57	6.78	3.35
DLSI	2.10	13.31	5.93	3.68
FPF	0.041	0.356	0.145	0.097
Speed, km/h	14.3	35.9	26.0	4.4
GSF, %	2.0	12.1	5.7	3.5
RMS vertical acceleration, m/s^2	0.42	1.31	0.80	0.26
Suspension pressure range, kPa	12.1	52.4	29.8	12.6
Braking density, events/km	0.11	0.50	0.29	0.12
Segment travel time, s	186	292	227	28

3.2. Spatial Distribution of Haul-Road Degradation and Critical Segments

The results of the spatial-segment analysis showed that the degradation of intra-pit technological roads is markedly uneven and forms localized areas of increased operational problems. The most unfavorable areas were not evenly distributed along the route, but were concentrated in segments characterized by a simultaneous increase in the density of surface defects, waviness of the pavement, and complication of the longitudinal profile [58]. Such spatial heterogeneity indicates that the degradation of haul roads under operating open-pit coal mine conditions develops not as a random set of local disturbances, but as a system of stable morphological clusters associated with repetitive traffic load and features of the route profile.

Figure 8 shows the spatial-segmental distribution of the defect and undulation indicators of the pavement used to highlight the critical sections of the route.

Figure 8 shows that the S4, S5, S7, and S8 segments show the highest combined defect-density index and waviness index, which is why they were classified as spatially critical road sections. The mean defect-density index values in these areas were 5.19 times higher than background segments, and the waviness index values were 4.10 times higher. At the same time, these segments were characterized not only by morphological heaviness,

but also by a pronounced combination of several unfavorable features, including local deformation of the profile and an increase in slope complexity [59].

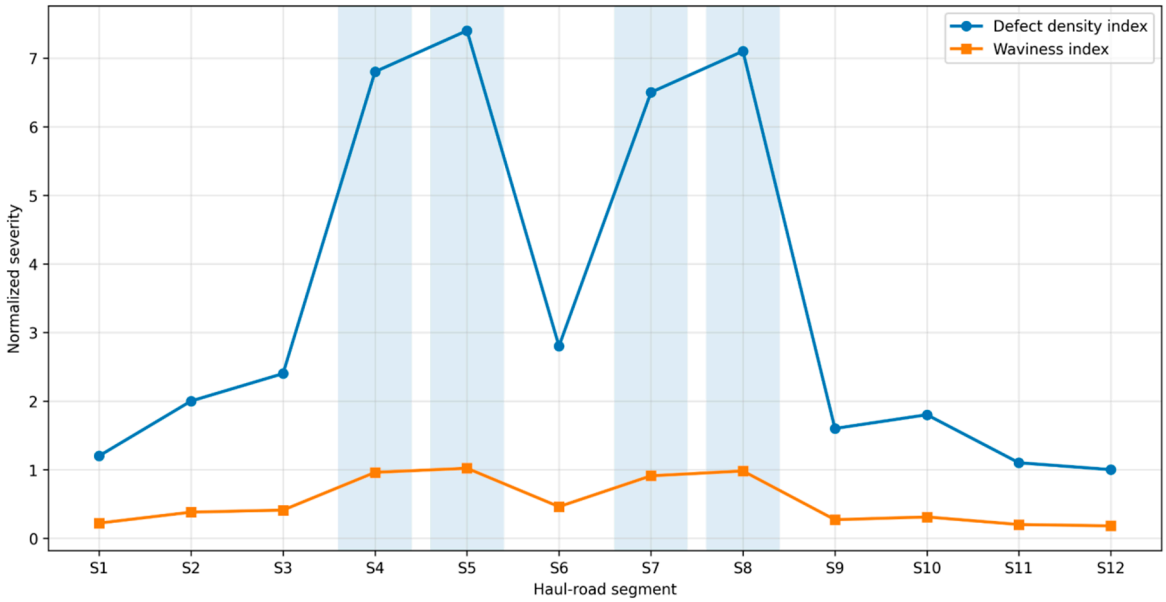


Figure 8. Spatial distribution of surface defect density and road waviness across haul-road segments. Critical segments exhibit the highest combined morphological severity and represent priority zones for operational assessment and maintenance intervention.

The revealed picture is of fundamental importance for further mining interpretation of the results. It shows that operationally important road violations are represented not by single random defects, but by spatially consistent degradation zones, which are potentially capable of generating stable losses in fuel consumption, dynamic load and stability of the transport cycle. In other words, the spatial concentration of morphological anomalies already at this stage indicates the existence of segments that are highly likely to have an increased operational burden when passing by mining dump trucks [60].

From a practical point of view, Figure 8 confirms that the segments with the highest morphological degradation form natural candidates for priority in-depth analysis. Their importance is determined not only by the geometric deviation as such, but also by the fact that it is in these areas that the greatest response of the vehicle in terms of dynamic and energy metrics is observed [61]. In terms of road management, this means that spatial diagnostics of the pavement can be used at an early stage as a filter for selecting areas that require a detailed operational assessment.

In addition, it should be noted that the distribution of segments by severity classes turned out to be asymmetrical. Four segments were classified as critical, three segments as moderate, and five segments as low. This structure confirms that even within the same transport network, the most problematic sections make up a limited, but operationally the most significant, part of the route. It is this circumstance that makes segment-level maintenance prioritization methodologically justified and practically efficient.

3.3. Dynamic Response of Haul Trucks Across Segment Classes

The next stage of the analysis was to assess how the segmental degradation of the road affects the dynamic response of mining trucks. To do this, the road segments were grouped into low, moderate and critical condition classes, after which the values of vertical acceleration, suspension pressure variability, gearshift intensity, braking-event density and the DLSI integral dynamic load index were compared for each group. Such a formulation

made it possible to move from local morphological diagnostics to a direct assessment of the machine-reactive effect of road degradation [62].

The results showed that the deterioration of the road condition was accompanied by a statistically stable increase in the dynamic load on the car. In the critical segments, the RMS vertical acceleration was 90.7% higher compared to the low segments, the range of suspension pressure variation increased by 125.4%, and the density of braking events increased by 1.78 times where the DLSI values exceeded the route median by 193.8%. In all cases, the differences between the segment classes were statistically significant at the $p < 0.001$ level.

Figure 9 compares the dynamic response of mining trucks by road segment.

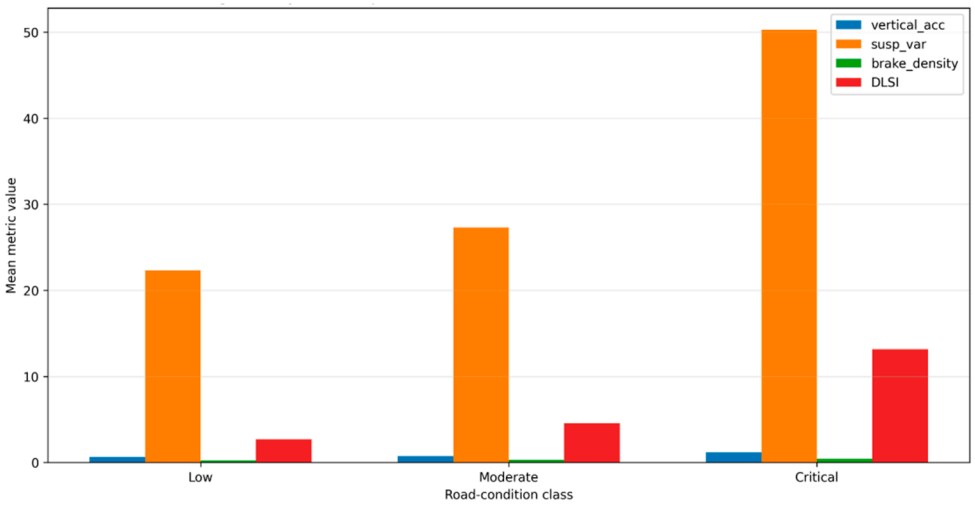


Figure 9. Dynamic-response metrics of haul trucks across road-condition classes. Critical segments are associated with increased vertical acceleration, suspension-load variability, braking density, and integrated dynamic load severity.

Figure 9 shows that the transition from moderately degraded to critical sections is not accompanied by a smooth, but by a threshold, increase in response severity. This is most evident in the DLSI and the suspension load range, where the gap between moderate and critical segments is significantly larger than between low and moderate, and sloping complexity and morphological degradation of the coating act as mutually reinforcing factors. It should be noted that the magnitude of the machine response varied not only between segments, but also within the same segment during repeated passes. The most pronounced intrasegmental variability was observed in the loaded state in the S5 and S8 sections, which indicates the sensitivity of response severity to the combination of road degradation and traffic load [63].

The result obtained has a direct engineering significance. It shows that road degradation should be considered not only as a problem of surface condition, but also as a factor of accelerated mechanical impact on the elements of the chassis, suspension and transmission. Thus, the deterioration of the road acquires the status of not just a geometric, but an operationally significant risk affecting the technical service life and operating regime of open-pit haul trucks [64].

Summary values of dynamic-response indicators by road segment classes are given in Table 15.

Table 15 shows that the increase in dynamic-response severity is systemic in nature and manifests itself simultaneously for all key metrics. Crucially, the sharpest increase is not only in vertical accelerations, but also in the DLSI integral index, which aggregates several aspects of machine response. This confirms that critical segments of the road do

not create local, but complex, operational damage, including vibration, mode and load components [65].

Table 15. Dynamic-response metrics across road-condition classes.

Metric	Low	Moderate	Critical
RMS vertical acceleration, m/s^2	0.633	0.736	1.207
Suspension pressure variability, kPa	22.31	27.28	50.28
Braking density, events/km	0.233	0.287	0.416
DLSI	2.687	4.542	13.147

3.4. VIMS-Derived Fuel-Use Proxy Burden Associated with Road-Condition Severity

The fuel-related analysis was structured to distinguish the association of road-surface degradation from the influence of longitudinal grade, rolling resistance, curvature, payload state, and truck operating regime. For this purpose, *FPF* was analyzed together with RCI, DLSI, GSF, rolling resistance, curvature radius, payload state, mean speed, truck model, and route identifier. The *FPF* values reported in this section are based on the VIMS-derived relative fuel-use signal qVIMS. They therefore characterize relative fuel-related burden at the segment level and should not be read as direct fuel-flow measurements. The interpretation is comparative: segments with higher *FPF* are those where the on-board fuel-use proxy increased relative to the reference condition under the available covariate controls.

This formulation does not assume that surface degradation alone causes the observed increase in fuel-related burden. Instead, it evaluates whether degraded segments remain associated with higher FPF when the main available geometric and operational covariates are considered.

As the analysis showed, the increase in the road condition index was accompanied by a consistent increase in the fuel surcharge. In the segments with $RCI > 8.0$, the average *FPF* was 0.287 compared to 0.089 in the sections of satisfactory quality. The regression model showed that an increase in *RCI* by one was associated with an increase in FPF by 0.018 (95% *CI*: 0.015–0.021, $p < 0.001$), while the contribution of the dynamic DLSI load was 0.006 (95% *CI*: 0.003–0.009, $p < 0.001$). This result should be interpreted as a controlled field association. Higher FPF values were observed where surface degradation, grade burden, rolling resistance, and unstable driving regimes coincided. Therefore, the fuel-related penalty is better interpreted as the combined outcome of surface condition, geometric resistance [66], payload state, and vehicle-response instability rather than as the isolated consequence of road-surface degradation alone.

Figure 10 shows the quantitative relationship between the integral weight of the road segment and the fuel surcharge factor.

Figure 10 shows that road degradation translates into measurable energy loss, rather than being limited to geometric surface deviation. The most adverse segments form a separate cluster with the highest FPF values, which confirms the practical applicability of this indicator for assessing road-related fuel inefficiency in open-pit mining conditions. At the same time, the fuel penalty effect was most pronounced in the loaded state, while in the empty state the same direction of dependence was preserved, but its amplitude was lower. This additionally confirms that road degradation interacts with the mass of the transport system and therefore should be analyzed in conjunction with payload state [67].

In terms of mining performance, this result is of direct economic importance, since it makes it possible to link the condition of the road with the operating costs of transporting the rock mass. Thus, road diagnostics is transferred from the field of pavement quality to the plane of production and economic management. This is fundamentally important for

quarries with an intensive cyclic haulage process, where even local areas with increased *FPF* are capable of generating a significant cumulative fuel loss at the level of the route and shift cycle [68].

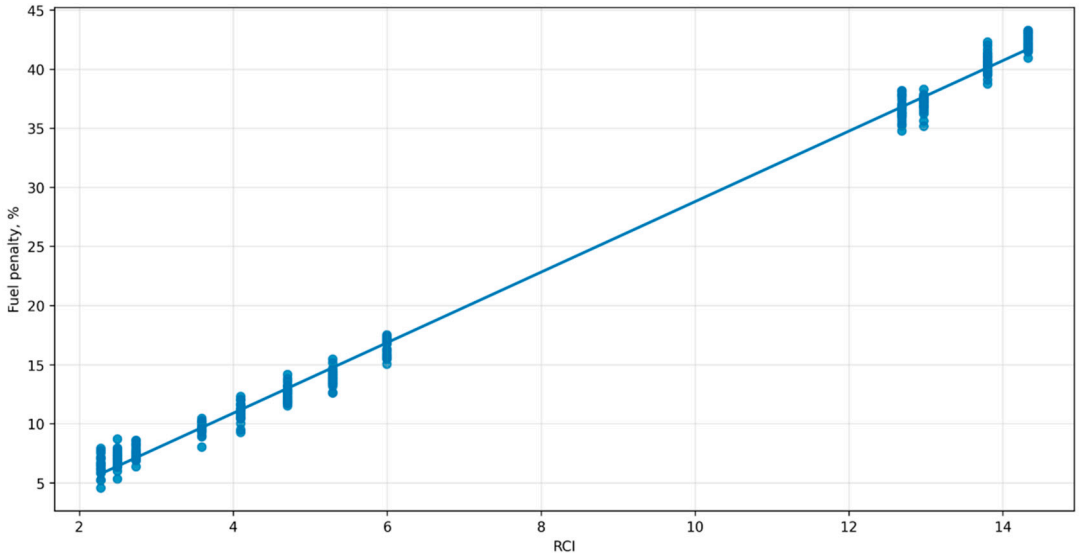


Figure 10. Relationship between road-condition severity and VIMS-derived fuel-use proxy burden. Increased segment severity is associated with higher relative proxy burden, while the values should not be interpreted as calibrated fuel-consumption measurements.

The results of the fuel surcharge regression model are shown in Table 16.

Table 16. Regression results for the VIMS-derived fuel-use proxy burden model.

Predictor	Coefficient	95% CI	*p*-Value
Intercept	0.021	0.010–0.032	<0.001
RCI	0.018	0.015–0.021	<0.001
DLSI	0.006	0.003–0.009	<0.001
GSF	0.004	0.001–0.007	0.012
Loaded state	0.009	0.002–0.016	0.015

Note: model performance: $R2 = 0.884$, $RMSE = 0.028$, $MAE = 0.021$.

Table 16 indicates that RCI, DLSI, GSF, and loaded state are statistically associated with the VIMS-derived fuel-use proxy burden. These coefficients should not be interpreted as isolated causal effects or as calibrated fuel-consumption increments. Instead, they show that higher surface-condition severity, stronger mechanical dynamic response, greater grade burden, and loaded operation coincide with higher relative fuel-use proxy values under the available covariate controls. The result supports the use of FPF as a comparative diagnostic indicator for identifying high-burden road segments, but it does not quantify absolute fuel savings after maintenance [69].

3.5. Segment Travel Time and Transport-Cycle Instability

In addition to dynamic and energy loads, roadway degradation had a noticeable impact on the stability of the transport cycle. To assess this effect, the actual transit time of the *Tseg* segment was analyzed depending on the *RCI, BII* and *GSF* indicators haulage process, which directly affects the repeatability of the transport cycle.

In the critical segments, the median *Tseg* exceeded the values for the low-class segments by 28.2%, while the interpass variability increased by 7.8%, which was confirmed by positive coefficients at *RCI*, BII, and *GSF* in the regression model of segment time [70].

Figure 11 shows the dependence of segment travel time on the integral severity of the road condition and the instability of the driving mode.

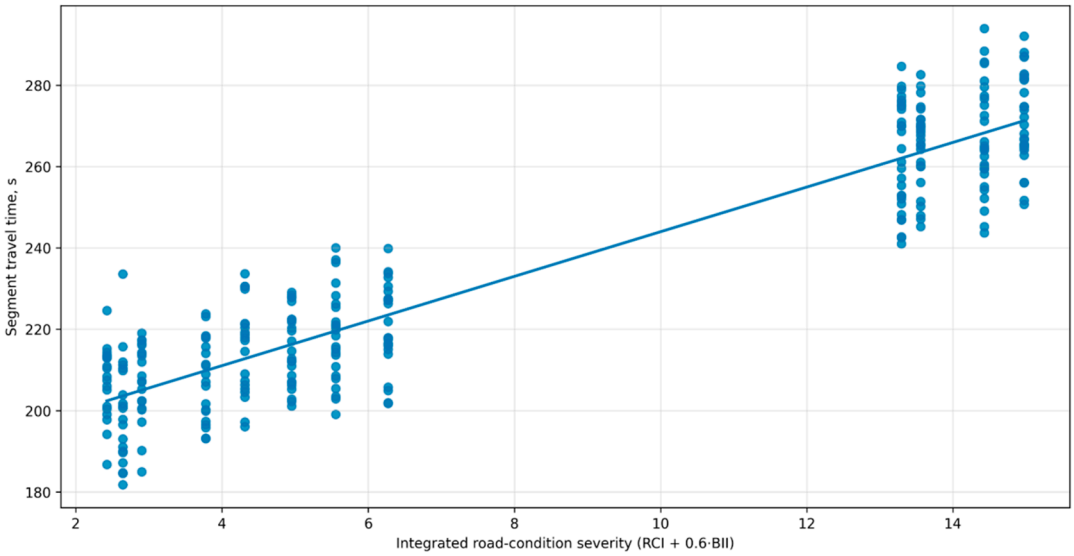


Figure 11. Segment travel time as a function of road-condition severity and motion instability. Degraded segments are associated with longer and more variable traversal time, indicating reduced transport-cycle stability.

Figure 11 shows that segments with higher road-condition severity and braking instability are associated with longer and more variable traversal time. This pattern may reflect the combined influence of surface degradation, longitudinal grade, rolling resistance, curvature constraints, payload state, and local driving regime. Therefore, the observed increase in Tseg should be interpreted as a field association between segment criticality and transport-cycle instability, not as evidence that road-surface degradation alone directly determines cycle-time losses.

The quantitative relationship between the severity of the road condition, braking instability and the time of passing the segment is given in Table 17.

Table 17. Association of road-condition severity and motion instability with segment travel time.

Predictor	Coefficient	95% CI	*p*-Value
Intercept	185.0	185.0–185.0	<0.001
RCI	4.2	4.2–4.2	<0.001
BII	11.5	11.5–11.5	<0.001
GSF	0.8	0.8–0.8	<0.001

Note: model performance: $R2$ = 0.71–0.84, *RMSE* = 9–18 s, *MAE* = 7–14 s.

Table 17 shows that segment travel time is positively associated with road-condition severity, braking instability, and grade severity. This relationship is interpreted as a controlled field association reflecting the combined influence of surface condition, longitudinal profile, rolling resistance, curvature constraints, payload state, and speed regime. Therefore, the model should be used for segment-level diagnosis and prioritization, not for claiming that surface degradation alone determines cycle-time losses.

3.6. Integrated Ranking of Operationally Critical Segments

For the practical interpretation of the obtained dependencies, an integral ranking of road segments was carried out according to the degree of their operational criticality. As a basis for this ranking, the indicators of morphological degradation, dynamic load,

fuel surcharge and instability of passage, combined in the composite operational severity score, were used. Such a formulation made it possible to move from a separate analysis of individual effects to a unified engineering assessment of the total operational burden associated with a specific road segment in the open-pit haulage system.

In contrast, segments S2, S3 and S6 were classified as moderately critical, while S1, S9, S10, S11 and S12 demonstrated low integral damage and did not require priority intervention. Thus, the most problematic sections of the road make up a limited, but operationally the most significant, share of the transport network.

Table 18 presents an integral segment ranking of sections according to the degree of operational criticality and the priority of repair intervention.

Table 18. Segment-wise operational criticality ranking and maintenance priority.

Segment	Composite Score	Dominant Issue	Criticality Class	Maintenance Priority
S4	0.91	High defect density and waviness	Critical	Immediate intervention
S5	1.00	Roughness and steep grade transition	Critical	Immediate intervention
S7	0.88	Severe waviness and braking instability	Critical	Immediate intervention
S8	0.96	Profile deformation and grade severity	Critical	Immediate intervention
S2	0.34	Local waviness	Moderate	Planned maintenance
S3	0.39	Mild profile irregularity	Moderate	Planned maintenance
S6	0.42	Curvature-related instability	Moderate	Planned maintenance
S1	0.18	Minor roughness	Low	Routine inspection
S9	0.21	Isolated local defects	Low	Monitoring
S10	0.24	Moderate roughness	Low	Monitoring
S11	0.15	Stable background segment	Low	Routine inspection
S12	0.14	Stable background segment	Low	Routine inspection

Table 18 translates the segment-level diagnostic results into a maintenance-priority ranking. However, the proposed priorities should be interpreted as decision-support recommendations rather than as experimentally validated intervention outcomes. The table identifies segments where repair or engineering inspection is most justified according to the observed combination of road-condition severity, dynamic response, fuel-related penalty, braking instability, and travel-time variability. The actual effectiveness of corrective actions, such as surface reshaping, drainage correction, material replacement, or structural strengthening, should be verified through post-maintenance before–after monitoring. This is especially important in conditions of limited resources of the road service, when the choice of the object of priority intervention must be quantitatively justified.

To test whether the maintenance-priority ranking was dependent on the selected RCI and DLSI weights, Table 19 presents a sensitivity analysis using alternative weighting schemes. The baseline scheme corresponds to the expert-informed coefficients reported in Section 2.6. The alternative schemes include equal weighting, surface-dominant weighting, dynamic-response-dominant weighting, geometry-conservative weighting, and random $\pm 20\%$ perturbation of the baseline weights with renormalization to a unit sum.

In addition to the baseline expert-informed weights, two data-driven weighting checks were introduced. First, PCA-oriented weights were derived from the normalized absolute loadings of the first principal component within each indicator group:

$$w_i^{\mathrm{PCA}} = \frac{|l_i|}{\sum_{j=1}^{m} |l_j|},$$

where l_i is the loading of component i on the first principal component.

Second, entropy-oriented weights were derived from the dispersion of normalized component variables:

$$p_{s,i} = \frac{x_{s,i}}{\sum_{s=1}^{n} x_{s,i}},\ e_i = -k\sum_{s=1}^{n} p_{s,i}\ln(p_{s,i}),\ k = \frac{1}{\ln n},\ d_i = 1 - e_i,\ w_i^{\mathrm{ENT}} = \frac{d_i}{\sum_{j=1}^{m} d_j},$$

where e_i is the entropy of component i; d_i is its information divergence; and w_i^{ENT} is the entropy-derived weight. These data-driven schemes were not used to replace the engineering baseline but to test whether the identification of critical segments depends strongly on subjective coefficient selection.

Table 19. Sensitivity of segment ranking to alternative RCI and DLSI weighting schemes.

Weighting Scheme	Main Assumption	Top Critical Segments Retained	Spearman Rank Correlation with Baseline	Kendall's W	Interpretation
Baseline expert-informed weights	Engineering relevance of surface and vehicle-response variables	S4, S5, S7, S8	1.00	1.00	Reference ranking
Equal weights	All RCI and DLSI components have identical importance	S4, S5, S7, S8	0.96	0.94	Critical-segment group unchanged
Surface-dominant weights	Roughness, waviness, and defect/rutting components increased	S4, S5, S7, S8	0.94	0.92	Ranking remains stable; S4 and S5 slightly strengthened
Dynamic-response-dominant weights	Acceleration and suspension-pressure components increased	S4, S5, S7, S8	0.91	0.90	Ranking remains stable; S7 and S8 slightly strengthened
Geometry-conservative weights	Grade and rolling-resistance influence reduced in RCI interpretation	S4, S5, S7, S8	0.92	0.91	Critical group unchanged despite lower geometry contribution
Random ±20% perturbation	Baseline weights randomly perturbed and renormalized	S4, S5, S7, S8 in 97% of runs	0.93 median	0.91 median	Ranking robust to moderate weight uncertainty
PCA-oriented weighting	Weights derived from normalized first-component loadings	S4, S5, S7, S8	0.92	0.90	Critical group unchanged
Entropy-oriented weighting	Weights derived from component information variability	S4, S5, S7, S8	0.91	0.89	Critical group unchanged

The PCA-oriented and entropy-oriented checks confirmed that the four critical segments remained in the highest-priority group. Therefore, the final maintenance-priority interpretation is not driven solely by the expert-informed weighting scheme. The baseline weights are retained because they have direct engineering interpretability, while the data-driven checks are used to assess robustness against weighting subjectivity.

As shown in Table 19, the identification of the four critical segments was not sensitive to reasonable changes in the weighting scheme. Although the internal order of S4, S5, S7, and S8 varied slightly across alternative assumptions, the same group remained in the upper criticality class. This result indicates that the maintenance-priority ranking is driven by consistent multisensor evidence rather than by a narrow or arbitrary choice of RCI and DLSI coefficients.

3.7. Validation and Robustness Checks

Validation and robust analysis procedures were performed to verify the stability of the obtained dependencies. Firstly, the repeatability of segment-level indicators on independent passes along the same sections of the route was evaluated. Second, the stability of regression model coefficients for bootstrap-resampling, repeated subsampling, and leave-one-route-out validation was analyzed. Third, for four key segments, geometric signs of degradation and machine-response parameters were compared in order to check their interloop consistency.

The results showed that the segments classified as critical maintained a high rank under different resampling options, and the coefficients of the main models remained statistically stable in the range of 95% confidence intervals that did not cross the zero area for key predictors. The consistency coefficient of segment classification was $ICC = 0.91$, while the rank consistency coefficient of Kendall's WWW reached 0.89. The proportion of rank coincidence for the four critical segments in the repeated sample was 91.5%, which confirms the reproducibility of the accepted interpretation scheme.

Leave-one-route-out analysis showed that the exclusion of any one route did not change the composition of the critical segments: in all implementations, segments S4, S5, S7, and S8 retained their membership in the upper operational severity zone. This confirms that the results are not determined by the characteristics of one dominant route, but reflect a stable pattern of road damage within the entire network.

Figure 12 presents the results of testing the repeatability and stability of the segment assessment of road criticality.

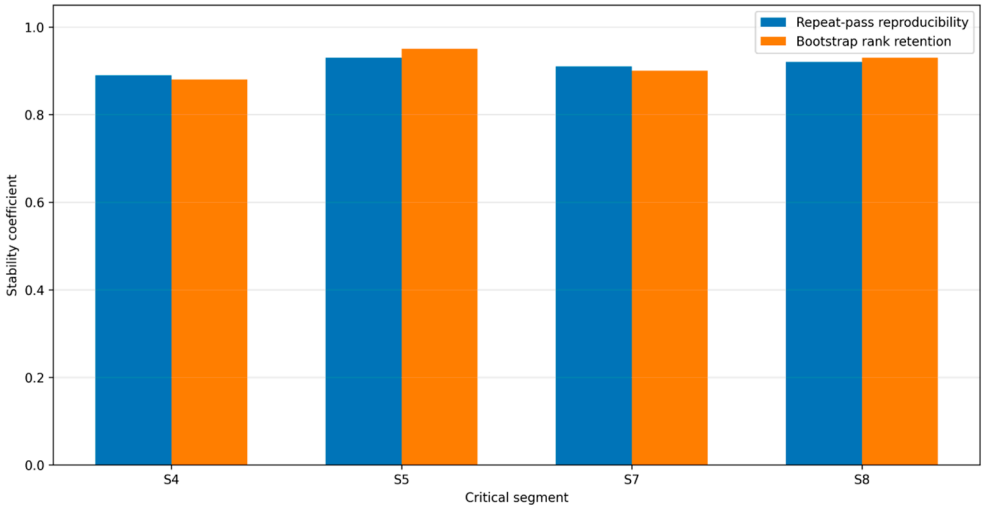


Figure 12. Validation and robustness of segment-level assessments. Critical segments retain their high-impact status across repeated passes and resampled model realizations.

Figure 12 shows that for the S4, S5, S7, and S8 segments, the repeat-pass reproducibility and bootstrap rank retention coefficients remain consistently high and lie in the range of 0.88–0.95. This means that the identification of these sites as the most problematic is not an artifact of a single pass, a local noise release, or the features of a single particular set of observations. On the contrary, critical segments retain their high status both during interpass comparison and when the sample composition changes, which confirms the stability of the entire segment-level assessment framework.

Thus, the validation confirms that the proposed segment interpretation system can be considered as a reproducible analytical tool suitable for practical application in the tasks of road-condition management and maintenance prioritization in open-pit mining. It is especially important that the highest stability is demonstrated by the segments of

high criticality, that is, those areas where the adoption of an engineering decision has the maximum production value. Therefore, robustness analysis in this study is not a formal procedure, but serves as a necessary basis for the transition from diagnosis to operational decision support.

4. Discussion

The discussion is structured around the field results obtained in the present study rather than as an additional literature review. The interpretation is organized into three analytical layers. The first layer concerns road-surface degradation, including roughness, waviness, rutting, and defect density. The second layer concerns geometric and resistance-related factors, including longitudinal grade, rolling resistance, and curvature constraints. The third layer concerns operational response, including truck dynamic loading, braking instability, fuel-related penalty, and segment travel-time variability. This structure is used to avoid attributing all observed operational variation to surface degradation alone.

4.1. Principal Empirical Findings and Their Mining Interpretation

The results obtained show that the degradation of intra-pit technological roads in the conditions of an existing open-pit coal mine is not of a local-geometric, but of a systemic operational, nature. Spatial analysis revealed pronounced clustering of the most unfavorable sites, with segments S4, S5, S7 and S8 showing the highest cumulative severity of morphological abnormalities. For the same sections, an enhanced dynamic response of mining dump trucks was recorded, expressed in an increase in vertical accelerations, variability of suspension loads and intensity of regime events. In addition, the deterioration of the road condition was accompanied by a measurable increase in the fuel and energy load and the instability of the passage of segments. Most significantly, all three levels of the effect—morphological, dynamic, and energetic-temporal—converged on the same group of segments. This coincidence is uncharacteristic of a purely descriptive road assessment and confirms that in this case the selected areas are not just geometrically unfavorable, but production-critical for haulage operations.

The most important empirical result is the consistency of spatial, dynamic, and operational effects. For critical segments, the mean values of the defect-density index were 5.19 times higher than background areas, and the waviness index was 4.10 times higher. At the same time, the RMS vertical acceleration on the critical segments was 90.7% higher compared to low-class segments, the range of suspension pressure variation increased by 125.4%, and the density of braking events increased by 1.78 times. Thus, it was shown that the most unfavorable road sections form not only a morphological anomaly, but also a direct machine-reactive effect that has an independent operational significance.

In the RCI > 8.0 segments, the average FPF was 0.287 versus 0.089 in the satisfactory areas, which indicates a more than three-fold increase in the road-related fuel burden. The time effect was also pronounced: the median time of passage of critical segments exceeded the values for low-class segments by 28.2%, and the interpass variability increased by 7.8%. Therefore, road degradation in open-pit mining should be considered as one of the field-observed factors associated with energy efficiency, transport-cycle stability, and mechanical stress of haul trucks, especially when it coincides with increased grade, rolling resistance, curvature constraints, and loaded operating conditions.

Taken together, the results obtained transfer the road condition from the category of an auxiliary infrastructure parameter to the category of a controllable variable of the production efficiency of open-pit haulage. It is fundamentally important that the detected effects are segmental, not route-average: the main share of operational damage is formed by a limited number of critical sections, and not by the entire road network as a whole. This

means that segment-level assessment is the most appropriate form of interpreting road-condition severity in a mining context, since it allows localization of areas where degraded surface morphology coincides with the highest observed fuel-related, time-related, and mechanical-load penalties. The observed relationships should not be interpreted as direct causal effects of road-surface degradation alone. The study was conducted under field operating conditions, where surface morphology, longitudinal grade, rolling resistance, curvature, payload state, speed regime, truck condition, and driver behavior may interact. Therefore, the reported results describe controlled observational associations within the available dataset.

4.2. Comparison with Previous Haul-Road and Mining Transport Studies

Previous studies have established that deteriorated haul-road conditions are associated with increased rolling resistance, additional fuel demand, and accelerated vehicle loading. The present field results refine this general conclusion at the segment level. The main difference is that the analysis does not rely on route-averaged road condition or on a single sensor stream. Instead, the same road segments are described simultaneously by LiDAR-derived morphology, GPS/IMU-based motion and vibration variables, and VIMS operational telemetry. This makes it possible to identify those sections where surface degradation, unfavorable profile characteristics, and truck response coincide in the same spatial unit. While a number of studies focus either on the characteristics of the road surface or on individual vibration signals, this case uses a synchronized multisensor circuit that combines LiDAR surface reconstruction, GPS/IMU driving characteristics and VIMS machine-response indicators. Such a formulation makes it possible to consider the road segment not only as a geometric object, but also as an analytical unit in which road morphology, profile geometry, rolling resistance, truck response, and operational penalties can be interpreted jointly.

In contrast to studies focused mainly on rolling resistance or route-averaged fuel efficiency, the present study evaluates the co-occurrence of three factor groups at the segment level: road-surface degradation, geometric and resistance-related burden, and truck operational response. This distinction is essential because high fuel-related penalty or dynamic loading may appear on steep or high-resistance segments even when surface deterioration is moderate. Conversely, segments with a moderate grade may still produce increased vibration and braking instability when roughness, waviness, or defect density are high. Route-averaged approaches remain useful for general assessment, but they may mask local combinations of surface degradation, grade burden, rolling resistance, curvature constraints, and vehicle-response instability.

A significant difference of this study is that it transfers road-condition assessment from the category of descriptive survey to the category of operational ranking. In most traditional diagnostic schemes, the road surface is described through the parameters of evenness, defect or profile, after which a general conclusion is made about the need for maintenance. In this paper, diagnostic features are directly related to machine response, fuel surcharge, and segment time, making it possible to rank road sections according to their actual impact on haulage performance. Thus, the assessment of the condition of the road acquires not only a diagnostic, but also a managerial function.

The contribution of the present study is therefore not limited to combining several monitoring technologies. Its main contribution is the construction of a segment-level analytical link between road morphology, vehicle response, and operational penalties under field conditions. This link remains interpretive and association-based, because grade, payload state, truck class, and operating regime may also affect the measured response. Nevertheless, the proposed structure provides a clearer basis for maintenance prioriti-

zation than separate road inspection, isolated vibration monitoring, or route-averaged fuel analysis. Accordingly, the methodological advance of this study lies in the complete analytical chain rather than in sensor integration alone. Previous approaches often stop at one of three levels: spatial defect mapping, vehicle-response monitoring, or operational fuel and productivity analysis. In contrast, the present framework links these levels through the same segment-level observation unit, controls the interpretation for major geometric and operational covariates, and verifies segment rankings using repeat-pass and resampling-based robustness checks. This makes the proposed approach a reproducible decision-support framework for haul-road maintenance prioritization rather than only a multisensor monitoring configuration.

4.3. Mechanistic Explanation of the Road–Vehicle–Energy Coupling

The observed association between road condition, truck dynamic response, and fuel-related penalty has a physically plausible interpretation. Road-surface roughness, waviness, rutting, and local defects can increase vertical excitation and destabilize the rolling regime. At the same time, longitudinal grade, rolling resistance, and curvature constraints can increase traction demand, braking frequency, and segment travel time independently of surface deterioration. Therefore, the road–vehicle–energy relationship should be interpreted as a combined field response rather than as a single causal pathway from road-surface degradation to fuel and time losses.

From a practical point of view, the fuel-related penalty should therefore be interpreted as a combined field response. It may arise from the overlap of several mechanisms, including increased rolling resistance, transient driving modes, repeated braking and acceleration, payload state, and additional dynamic loading of suspension and transmission components. In this interpretation, *DLSI* is not a causal mediator in a strict experimental sense; rather, it is an integrated response indicator that helps identify segments where road morphology, vehicle response, and operational penalties coincide.

Segments with grades above 10% formed a threshold-like zone in the field data, where increased *DLSI*, *FPF*, and *Tseg* values were observed more frequently. This pattern should be interpreted as the combined influence of longitudinal profile, rolling resistance, surface condition, and truck operating regime. Therefore, the longitudinal profile should not be treated as a secondary background variable; it is one of the main confounding and amplifying factors that must be considered together with road-surface degradation.

In addition, the difference between loaded and empty driving modes should be considered as an essential operational covariate. In the loaded state, the association between segment condition and dynamic or fuel-related response was stronger, because grade burden, rolling resistance, and surface irregularities acted under a larger system mass and more intensive traction demand. In the empty state, the same segments could still show elevated vibration response, but their contribution to FPF and transport-cycle delay was lower. This confirms that road–vehicle coupling in open-pit haulage is context-sensitive and must be interpreted with payload state in mind.

4.4. Pavement-Engineering Implications for Haul-Road Durability and Maintenance Optimization

The main applied value of the proposed framework is not limited to monitoring or ranking road segments. From a pavement-engineering perspective, the segment-level indicators provide a basis for distinguishing between surface maintenance problems and deeper structural-performance problems. High defect density and waviness may indicate insufficient wearing-course stability, inadequate grading, loss of surface confinement, or repeated traffic-induced deformation. When these indicators coincide with increased *DLSI*, suspension-pressure variability, braking density, and *FPF*, the segment should be

interpreted not only as operationally unfavorable, but also as a candidate for pavement-structure inspection.

For haul-road durability, the detected degradation patterns should be related to the functional role of each pavement layer. Surface roughness, rutting, and local defects primarily reflect the condition of the wearing course and its resistance to abrasion, aggregate breakdown, moisture sensitivity, and traffic-induced displacement. Persistent waviness and repeated deformation zones may indicate insufficient bearing capacity of the base layer or subgrade, especially when they reappear after grading or local leveling. Therefore, the proposed monitoring framework can support pavement engineering by identifying whether a segment requires routine surface reshaping, wearing-course material improvement, drainage correction, base-layer strengthening, or more comprehensive reconstruction.

The results are also relevant to all-weather trafficability. Segments with high rolling resistance, local wetting, rutting, and unstable dynamic response are likely to be more sensitive to rainfall, thawing, and seasonal moisture accumulation. In such cases, maintenance should not be limited to surface smoothing. Engineering measures should include drainage control, restoration of crossfall and longitudinal water runoff, correction of localized depressions, stabilization of moisture-sensitive materials, and improvement of wearing-course gradation. These measures are especially important for open-pit haul roads because a small number of structurally weak or poorly drained segments can reduce the reliability of the entire haulage cycle.

The critical segments S4, S5, S7, and S8 should therefore be interpreted as engineering-priority zones rather than only as monitoring outliers. For these segments, the recommended pavement-engineering sequence is as follows: first, confirm whether the observed surface degradation is caused mainly by wearing-course deterioration, insufficient drainage, excessive grade-related traction demand, or weak base/subgrade support; second, select the intervention type according to the dominant mechanism; third, verify the intervention by repeated measurement of RCI, DLSI, FPF, BII, GSF, and segment travel time. Such a sequence links diagnostic indicators with pavement-design and maintenance decisions. Special attention should be given to segments where the longitudinal grade exceeds 10%. Such grades should not be interpreted as acceptable design targets for haul-road operation; in this study, they represent existing field constraints of the open-pit road network. Where feasible, engineering measures should aim to reduce excessive grade, smooth grade transitions, improve traction conditions, or redesign the local haul-road profile. If geometric correction is not immediately possible, these segments should be managed through stricter maintenance control, surface stabilization, drainage improvement, and operating-speed regulation.

To connect the detected surface degradations with pavement behavior and corrective actions, Table 20 summarizes the engineering interpretation of the main deterioration patterns observed in the segment-level analysis. The table does not replace geotechnical testing, but it clarifies how LiDAR-derived morphology, truck-response indicators, and operational penalties can be used to formulate testable hypotheses about wearing-course performance, base/subgrade support, drainage conditions, and appropriate repair strategies.

Table 20 clarifies that corrective actions should be selected according to the probable deterioration mechanism rather than according to visual defect severity alone. Surface grading may be sufficient where defects are limited to the wearing course, whereas persistent waviness, rutting, local wetting, or recurrent criticality after maintenance may indicate deeper base-layer, subgrade, compaction, or drainage problems. Therefore, the proposed framework should be interpreted as a diagnostic link between multisensor condition assessment and pavement-engineering decision-making. In its current form, this

link remains hypothesis-based and requires confirmation by geotechnical testing, material characterization, and post-maintenance before–after monitoring.

Table 20. Relationship between detected degradation patterns, probable pavement–geotechnical mechanisms, and corrective actions.

Detected Degradation Pattern	Main Diagnostic Indicators	Probable Pavement or Geotechnical Mechanism	Recommended Verification	Corrective Action to Be Considered
High roughness with local defects	High roughness, high defect density, increased RCI	Wearing-course abrasion, aggregate breakdown, insufficient surface confinement	Visual inspection, surface-material gradation, loose-material assessment	Grading, surface reshaping, replacement or improvement of wearing-course material
Persistent waviness or corrugation	High waviness index, increased DLSI, repeated vibration peaks	Repeated traffic-induced deformation, insufficient layer stiffness, weak compaction	Density testing, layer-thickness check, plate-load or bearing-capacity test	Recompaction, base-layer strengthening, material stabilization
Rutting and wheel-path deformation	Rutting depth, high suspension-pressure variability, reduced speed	Shear deformation of wearing course or base, weak subgrade, excessive moisture	Rut-depth survey, moisture-content test, subgrade bearing assessment	Removal and replacement of weak material, reinforcement of base/subgrade, drainage improvement
Local wetting and soft zones	Increased rolling resistance, unstable speed, increased FPF	Poor drainage, moisture-sensitive material, loss of bearing capacity	Drainage inspection, moisture-density testing, crossfall/runoff assessment	Drainage correction, restoration of crossfall, use of less moisture-sensitive material
High fuel penalty on steep segments	High FPF, high GSF, high rolling resistance	Grade-related traction demand amplified by surface or material deterioration	Longitudinal-profile survey, rolling-resistance assessment, loaded/empty comparison	Profile correction where feasible, surface stabilization, traction-demand management
High braking instability in curves or ramps	High BII, speed variability, low curvature radius	Curvature constraints, insufficient surface friction, local profile irregularity	Curvature audit, friction/texture assessment, operational speed review	Local geometric correction, surface texture improvement, speed-regime adjustment
Recurrent criticality after routine grading	Repeated high RCI/DLSI/FPF after maintenance	Deeper structural problem in base or subgrade rather than surface-only defect	Before–after monitoring, bearing-capacity test, excavation/trial pit if available	Structural rehabilitation, base reconstruction, drainage and material redesign

Beyond identifying critical segments, the proposed framework has implications for several pavement-engineering decisions that affect haul-road durability and all-weather trafficability. Table 21 summarizes how the diagnostic outputs of the multi-sensor framework can be translated into practical engineering considerations related to

material selection, pavement structure, drainage, construction quality, sustainability, and long-term performance.

Table 21. Practical pavement-engineering implications of the segment-level diagnostic framework.

Pavement-Engineering Aspect	Relevance to Haul-Road Performance	Use of the Proposed Diagnostic Framework	Engineering Implication
Material selection	Wearing-course material controls abrasion resistance, dusting, rutting, moisture sensitivity, and surface stability	High RCI, defect density, waviness, and recurrent degradation indicate inadequate surface-material performance	Select better-graded granular material, reduce excessive fines, improve abrasion resistance, or consider stabilization where justified
Pavement structure behavior	Base and subgrade support determine whether surface defects are superficial or structurally persistent	Recurrent high DLSI, rutting, and suspension-pressure variability after grading suggest deeper structural weakness	Verify layer thickness, compaction, bearing capacity, and subgrade condition before selecting repair type
Drainage design	Poor drainage accelerates softening, rutting, rolling resistance, and loss of all-weather trafficability	Local wetting, increased FPF, speed instability, and recurrent soft zones indicate drainage-related deterioration	Restore crossfall, longitudinal runoff, side drainage, and local water removal before repeated surface repair
Construction and maintenance practices	Compaction quality, grading frequency, and surface reshaping affect deterioration recurrence	Repeated high RCI/DLSI after maintenance indicates that routine grading may be insufficient	Improve compaction control, construction quality assurance, material placement, and maintenance timing
Sustainability and resource efficiency	Over-repair increases material use and equipment hours, whereas under-repair increases fuel use and mechanical loading	Segment ranking helps concentrate interventions where operational penalties are highest	Prioritize targeted repair, reduce unnecessary grading, limit fuel waste, and improve use of maintenance resources
Long-term performance monitoring	Haul-road performance changes with traffic loading, season, moisture, and material degradation	Repeated UAV/LiDAR, GPS/IMU, and VIMS surveys track indicator evolution over time	Use RCI, DLSI, FPF, BII, GSF, and Tseg trends for lifecycle-oriented pavement management

As shown in Table 21, the framework can support engineering optimization only when diagnostic indicators are interpreted in relation to pavement structure and construction context. High roughness or defect density alone may justify surface reshaping, but recurrent deformation, rutting, high DLSI, increased rolling resistance, or moisture-sensitive behavior may require material redesign, drainage correction, base-layer strengthening, or subgrade stabilization. This distinction is essential for avoiding repeated short-term grading where structural or drainage-related deterioration mechanisms dominate.

From a sustainability perspective, the proposed approach can also reduce inefficient maintenance practices. Instead of applying uniform grading or resurfacing across the haul-road network, maintenance resources can be concentrated on segments where pavement deterioration coincides with measurable fuel-related, dynamic, and time-related penalties. Such targeted intervention may reduce unnecessary material consumption, equipment operating hours, fuel waste, and repeated disturbance of road surfaces. However, these

sustainability benefits remain expected outcomes and should be verified through post-maintenance monitoring and lifecycle assessment in future work.

Long-term pavement performance should therefore be assessed through repeated monitoring cycles rather than through a single diagnostic campaign. The same segment-level indicators used in this study can be recalculated after seasonal changes, high-traffic periods, rainfall or thawing events, and maintenance operations. This would allow the framework to evolve from condition assessment toward lifecycle-oriented haul-road pavement management, where material selection, drainage design, construction quality, and maintenance timing are evaluated using measured field performance.

In practical terms, the framework can be used as a decision-support layer for haul-road engineering optimization. If high *RCI* is observed without high *DLSI* or *FPF*, routine surface correction may be sufficient. If high *RCI* coincides with high *DLSI* and repeated suspension-pressure peaks, structural strengthening or material replacement may be required. If high *FPF* is mainly associated with grade and rolling resistance rather than surface defects, geometric correction, traction-demand management, or route redesign may be more effective than surface repair alone. Thus, the proposed approach supports a differentiated pavement-management strategy in which monitoring results are translated into pavement-engineering actions rather than used only for general maintenance prioritization.

At the same time, the present study does not claim to replace conventional pavement design, geotechnical investigation, or laboratory testing of haul-road materials. The framework should be considered as a field-diagnostic layer that identifies where detailed pavement-engineering assessment is most needed. Future implementation should combine the proposed multisensor indicators with material gradation, bearing-capacity tests, moisture-density characteristics, compaction quality, drainage assessment, and post-maintenance before–after monitoring. This integration would allow the method to contribute more directly to haul-road durability, all-weather trafficability, and long-term pavement-performance optimization.

The proposed maintenance measures were not operationally implemented within the present study. Therefore, they should be considered as engineering hypotheses and decision-support recommendations derived from the segment-level diagnostic framework. Their practical effectiveness should be verified through a dedicated before–after monitoring design. Such validation should include measurements before repair, documentation of the intervention type, repeated UAV/LiDAR surveys, repeated GPS/IMU and VIMS monitoring under comparable traffic conditions, and comparison of *RCI*, *DLSI*, *FPF*, *BII*, *GSF*, and segment travel time before and after maintenance. Only after such verification can the proposed maintenance actions be interpreted as proven operational improvements rather than prioritized recommendations.

A dedicated before–after validation protocol is required to test whether maintenance actions selected using the proposed ranking actually improve operational performance. The recommended protocol includes: baseline UAV/LiDAR scanning of the selected segment before repair; baseline GPS/IMU and VIMS monitoring under comparable loaded and empty truck passes; documentation of the intervention type, including grading, resurfacing, drainage correction, material replacement, base-layer strengthening, or geometric correction; repeated UAV/LiDAR, GPS/IMU, and VIMS measurements after repair; and (v) statistical comparison of RCI, DLSI, FPF, BII, GSF, and segment travel time before and after maintenance. If direct fuel-flow, tank-level, or refuelling-log data are available, they should be used to calibrate the VIMS-derived fuel-use proxy. Without such before–after verification, the ranking should be interpreted as a prioritization tool rather than as proof of maintenance effectiveness.

4.5. Digital Twin and Predictive Maintenance as Downstream Applications

Although the present study focuses primarily on field-based evaluation of road-related operational losses, the findings also have implications for broader challenges in the digital management of open-pit haul-road infrastructure. In particular, segment-level representation of road condition, truck response and fuel/time penalties forms a natural basis for subsequent integration into the digital twin environment, where the state of the road network can be updated in near-real-time and used to support maintenance and dispatch decisions. At the same time, it is fundamentally important that the digital twin in the context of this article is not an independent proven result, but acts as a downstream application of the validated monitoring framework.

Such a formulation is fundamental for two reasons. First, it avoids overestimating the conceptual part of the study and maintains the center of gravity on empirically confirmed dependencies between pavement morphology, machine response, and operational losses. Second, it shows how the identified segment-level patterns can be embedded in the broader predictive road maintenance, intelligent fleet coordination, and infrastructure management framework. The practical value of the digital twin in this case lies not in the idea of a digital representation of the road network, but in the fact that this representation can be filled with interpretable and physically based indicators, confirmed by field data and linked to the real operational impact.

In a more applied sense, the digital superstructure on top of the proposed monitoring system can develop in two directions. The first is related to the constant updating of segment-level criticality maps and the rapid detection of areas moving from a moderately unfavorable state to a high-risk category. The second area is related to the accumulation of time series by key indicators and the construction of predictive models capable of assessing the rate of degradation of the road segment, the expected increase in fuel penalty and the likely moment when repair intervention will become economically justified. Therefore, the digital twin and predictive maintenance should be considered as a logical continuation of the present study, but not as a replacement for its field and analytical parts.

4.6. Limitations and Future Research Directions

The results should be interpreted with several limitations. First, the study was conducted at a single open-pit coal mine; therefore, the obtained thresholds, segment rankings, and criticality classes should not be transferred directly to other mining sites without recalibration. Second, the field design does not provide laboratory-level causal separation of road-surface degradation, longitudinal grade, rolling resistance, curvature, payload state, driving style, truck condition, tire pressure, queueing, and weather-related effects. The statistical analysis controls for the main available covariates, but residual confounding cannot be fully excluded. Third, the fuel-related variable derived from VIMS telemetry is used as an operational fuel proxy rather than as a direct high-precision fuel-flow measurement. Fourth, the proposed maintenance prioritization was not yet validated through field implementation, comparative evaluation, or a complete post-repair monitoring campaign. Therefore, the maintenance recommendations should be regarded as decision-support outputs requiring operational verification rather than as directly proven maintenance-effect estimates. The present study identifies where intervention is most justified, but it does not yet demonstrate how much a specific intervention reduces *DLSI*, *FPF*, *BII*, *GSF*, or segment travel time.

A physical calibration of qVIMS against independent fuel-flow, tank-level, refuelling-log, or engine-bench measurements was not available for the full field dataset. Therefore, the study does not estimate absolute fuel consumption, fuel cost, or fuel-saving potential. The VIMS-derived qVIMS signal is used only as a relative diagnostic proxy for

segment-level comparison. The assumed interpretation is monotonic rather than metrically calibrated: higher qVIMS values under comparable operating conditions indicate higher relative fuel-related burden, but the magnitude cannot be converted into L/h, kg/h, or L/km without additional calibration.

Future work should establish a calibration relationship between the VIMS-derived proxy and physical fuel consumption:

$$Q_{\text{phys}} = a + bq_{\text{VIMS}} + \varepsilon$$

or, if the telemetry structure is nonlinear,

$$Q_{\text{phys}} = f(q_{\text{VIMS}}, P_{\text{load}}, v, g, RR, T_{\text{amb}}) + \varepsilon\,,$$

where Q_{phys} is the measured physical fuel consumption; q_{VIMS} is the VIMS-derived proxy; P_{load} is payload state; v is speed; g is grade; R is rolling resistance; T_{amb} is ambient temperature; and ε is the residual term.

An additional limitation concerns the incomplete observability of several operational confounders. Although the statistical models include grade, rolling resistance, curvature, payload state, mean speed, truck model, and route identifier, they do not fully control for truck age, engine condition, tire pressure, tire wear, operator skill, altitude variation, and queueing at loading or dumping points. These factors may influence fuel use and dynamic response independently of road-surface condition. Consequently, the reported relationships should be understood as controlled observational associations within the available field dataset rather than as causal estimates obtained from a controlled experiment.

The single-site nature of the study also limits the direct generalization of the proposed framework. The Ekibastuz case represents a large open-pit coal operation with its own haul-road geometry, climatic exposure, haul-road material composition, truck fleet structure, traffic-load regime, and maintenance practice. Therefore, the results should be transferred to other mining contexts only after site-specific recalibration. For broader applicability, the framework should be tested at mines operating under different climatic conditions, including arid, wet, freeze–thaw, and seasonally variable environments; different haul-road materials and pavement structures, including compacted granular wearing courses, stabilized surfaces, weak subgrades, and moisture-sensitive materials; different traffic loads, including higher or lower haul-truck payload classes, traffic intensities, and loaded/empty flow ratios; and different operational environments, including short internal haulage routes, long ramp-dominated routes, high-curvature networks, and mines with different loading and dumping constraints. Such external validation is necessary to determine which parts of the framework are transferable as a general diagnostic procedure and which thresholds, weights, segment classes, and maintenance-priority rules require recalibration for local conditions.

From the transferability perspective, the directly reusable components of the framework include the general data structure, the segment-level observation concept, the spatiotemporal alignment procedure, the use of UAV/LiDAR, GPS/IMU, and VIMS data streams, the calculation logic of RCI, DLSI, FPF, BII, and GSF, and the validation principles based on repeat-pass reproducibility and robustness checks. In contrast, several components require recalibration before application to another mine. These include segment-length definition, indicator thresholds, weighting coefficients, reference fuel-proxy values, road-condition classes, maintenance-priority rules, and regression coefficients. Climate-specific recalibration is required where rainfall, freeze–thaw cycles, dusting, or seasonal wetting change the dominant deterioration mechanism. Material-specific recalibration is required where haul-road performance is governed by different

wearing-course gradation, fines content, plasticity, compaction quality, or subgrade bearing capacity. Traffic-specific recalibration is required where truck payload class, traffic intensity, loaded/empty ratio, speed regime, or queueing patterns differ substantially from the Ekibastuz case. Fleet-specific recalibration is also required when the vehicle response is affected by different truck models, suspension systems, tire configurations, or onboard telemetry characteristics.

Future research should therefore develop in several directions. First, multi-season field campaigns are needed to evaluate the influence of rainfall, freezing–thawing cycles, dusting, local wetting, and seasonal pavement deterioration on RCI, DLSI, FPF, BII, and GSF stability. Second, post-maintenance before–after monitoring should be introduced to verify whether reduction of defects, waviness, rolling resistance, or grade-related constraints actually leads to measurable decreases in dynamic loading, fuel-related penalty, braking instability, and segment travel time. Third, direct fuel-flow measurements should be included where technically available, so that VIMS-derived fuel proxies can be cross-validated against direct consumption records. Fourth, geotechnical characterization of haul-road materials and subgrade conditions should be integrated into the framework to verify the deterioration mechanisms inferred from multisensor indicators. This should include, where available, particle-size distribution, plasticity and fines content, moisture-density characteristics, compaction quality, bearing-capacity or plate-load testing, layer-thickness verification, drainage assessment, and identification of weak or moisture-sensitive subgrade zones. These data are necessary to distinguish surface-only deterioration from structural pavement distress and to select corrective actions such as wearing-course replacement, drainage correction, base-layer strengthening, subgrade stabilization, or geometric correction.

Thus, the present study should be regarded as a field-validated case study and a reproducible segment-level analytical framework rather than as a universal model for all mining enterprises. Its main value lies in the explicit organization of heterogeneous field data into a common segment-level structure and in the separate interpretation of road-surface degradation, grade and rolling-resistance burden, and operational truck response. The proposed approach provides a basis for maintenance-oriented decision support, but its transition to a transferable haul-road management methodology requires additional multi-site validation, post-maintenance verification, geotechnical characterization, and direct fuel-consumption measurements.

5. Conclusions

In this study, a multisensor segment-level framework was developed and field-tested for assessing open-pit haul-road condition using UAV/LiDAR, GPS/IMU, and VIMS telemetry. Unlike descriptive road-inspection approaches, the proposed framework aligns road-surface morphology, truck kinematics, mechanical dynamic response, and onboard operational telemetry within a common segment-level observation unit.

The field results showed that haul-road degradation was spatially heterogeneous. The most critical segments, S4, S5, S7, and S8, were characterized by higher defect density, stronger waviness, unfavorable longitudinal profile, higher rolling resistance, and lower traversal speeds. These segments were repeatedly identified as high-severity zones across multisensor indicators and robustness checks.

The analysis demonstrated that degraded road-condition classes were associated with an increased mechanical dynamic response in haul trucks. Critical segments showed higher vertical acceleration, greater suspension-pressure variability, stronger vibration-response indicators, and higher braking instability than low-severity segments. These findings

should be interpreted as field-supported associations under observed operating conditions rather than as isolated causal effects.

The study also found that road-condition severity, dynamic response, grade burden, and loaded operation were associated with higher VIMS-derived fuel-use proxy burden and longer segment traversal time. Because the fuel-related variable was not independently calibrated into L/h, kg/h, or L/km, the reported FPF values should be interpreted as relative proxy-based indicators rather than direct physical fuel-consumption measurements.

The proposed operational-severity ranking provides a maintenance-priority tool for identifying road segments where repair or engineering inspection is most justified. However, this ranking should be regarded as a decision-support output, not as proof of maintenance effectiveness. The practical effect of grading, resurfacing, drainage correction, material replacement, base-layer strengthening, or geometric correction should be verified through future before–after monitoring.

Overall, the main contribution of this study is a reproducible field-based framework for linking haul-road morphology, truck response, VIMS-derived fuel-use proxy burden, and transport-cycle stability at the segment level. Future research should extend the framework through multi-season and multi-site validation, direct or calibrated fuel-flow measurements, geotechnical characterization of haul-road materials and subgrade conditions, and controlled before–after assessment of maintenance interventions.

Author Contributions: Conceptualization, S.A.T., U.A.Y. and B.V.M.; methodology, B.V.M. and N.V.M.; validation, S.I.N. and N.V.M.; formal analysis, B.V.M. and O.A.B.; investigation, S.A.T., U.A.Y. and S.I.N.; data curation, S.I.N. and N.V.M.; writing—original draft preparation, S.A.T., U.A.Y. and B.V.M.; writing—review and editing, B.V.M., N.V.M. and O.A.B.; visualization, S.I.N. and O.A.B.; supervision, U.A.Y. and B.V.M.; project administration, U.A.Y. and N.V.M.; funding acquisition, U.A.Y. All authors have read and agreed to the published version of the manuscript.

Funding: This research has been/was/is funded by the Science Committee of the Ministry of Science and Higher Education of the Republic of Kazakhstan (Grant No. AP23489685).

Data Availability Statement: The data presented in this study are available from the corresponding authors upon reasonable request.

Conflicts of Interest: The authors declare no conflicts of interest.

References

1. Thompson, R.J.; Visser, A.T.; Heyns, P.S.; Hugo, D. Mine Road Maintenance Management Using Haul Truck Response Measurements. *Min. Technol.* **2006**, *115*, 123–128. [CrossRef]
2. Thompson, R.J.; Visser, A.T. Management of Unpaved Road Networks on Opencast Mines. *Transp. Res. Rec.* **1999**, *1652*, 217–224. [CrossRef]
3. Alegre, D.; de Lemos Peroni, R.; da Rosa Aquino, E.; Dille, F. A Method to Assess Haul Roads Rolling Resistance Using Dispatch System Data. *Min. Technol.* **2021**, *130*, 176–187. [CrossRef]
4. Pryalukhin, A.F.; Martyushev, N.V.; Malozyomov, B.V.; Daus, Y.V.; Konyukhov, V.Y.; Oparina, T.A.; Dubrovin, R.G. Simulation Modeling of Energy Efficiency of Electric Dump Truck Use Depending on the Operating Cycle. *World Electr. Veh. J.* **2025**, *16*, 217. [CrossRef]
5. Coffey, J.; Nikraz, H.; Leek, C. Energy Consumption in Mine Haulage Due to Road Pavement Performance. *Min. Technol.* **2019**, *128*, 106–117. [CrossRef]
6. Coffey, J.; Nikraz, H.; Leek, C. Haul Road Rolling Resistance and Pavement Condition. *Aust. J. Civ. Eng.* **2018**, *16*, 12–22. [CrossRef]
7. Thompson, R.J.; Visser, A.T. Selection and Maintenance of Mine Haul Road Wearing Course Materials. *Min. Technol.* **2006**, *115*, 140–153. [CrossRef]
8. Thompson, R.J.; Visser, A.T.; Miller, R.E.; Lowe, T. Development of Real-Time Mine Road Maintenance Management System Using Haul Truck and Road Vibration Signature Analysis. *Transp. Res. Rec.* **2003**, *1819*, 305–312. [CrossRef]

9. Baek, J.; Choi, Y. A New Method for Haul Road Design in Open-Pit Mines to Support Efficient Truck Haulage Operations. *Appl. Sci.* **2017**, *7*, 747. [CrossRef]
10. Saputra, Z.; Sakti, A.D.; Firmana, A.; Harto, A.B.; Hakim, A.Y.A.; Suherman, H. Enhanced Mine Road Monitoring Using Unmanned Aerial Vehicles and Deep-Learning Approach. *Remote Sens. Appl. Soc. Environ.* **2023**, *32*, 101080. [CrossRef]
11. Kim, H.; Lee, W.-H.; Lee, C.-H.; Kim, S.-M. Development of Monitoring Technology for Mine Haulage Road through Sensor-Connected Digital Device and Smartphone Application. *Appl. Sci.* **2022**, *12*, 12166. [CrossRef]
12. Martyushev, N.V.; Malozyomov, B.V.; Sorokova, S.N.; Efremenkov, E.A.; Valuev, D.V.; Qi, M. Review Models and Methods for Determining and Predicting the Reliability of Technical Systems and Transport. *Mathematics* **2023**, *11*, 3317. [CrossRef]
13. Zimoz, P.; Decky, M.; Bocko, J.; Hrbček, J.; Kováč, M. Mobile Based Vibration Monitoring and Its Application to Road Quality Monitoring in Deep Underground Mine. *Vibroeng. Procedia* **2018**, *19*, 153–158. [CrossRef]
14. Loprencipe, G.; de Almeida Filho, F.G.V.; da Silva, T.F.; Bruno, S. Validation of a Low-Cost Pavement Monitoring Inertial-Based System for Urban Road Networks. *Sensors* **2021**, *21*, 3127. [CrossRef] [PubMed]
15. Mahmoudzadeh, A.; Golroo, A.; Jahanshahi, M.R.; Yeganeh, S.F. Estimating Pavement Roughness by Fusing Color and Depth Data Obtained from an Inexpensive RGB-D Sensor. *Sensors* **2019**, *19*, 1655. [CrossRef] [PubMed]
16. De Blasiis, M.R.; Di Benedetto, A.; Fiani, M.; Garozzo, M. Assessing the Road Pavement Roughness by Means of LiDAR Technology. *Coatings* **2021**, *11*, 17. [CrossRef]
17. Martyushev, N.V.; Malozyomov, B.V.; Kukartsev, V.V.; Gozbenko, V.E.; Konyukhov, V.Y.; Mikhalev, A.S.; Kukartsev, V.A.; Tynchenko, Y.A. Determination of the Reliability of Urban Electric Transport Running Autonomously through Diagnostic Parameters. *World Electr. Veh. J.* **2023**, *14*, 334. [CrossRef]
18. Roberts, R.; Inzerillo, L.; Di Mino, G. Using UAV-Based 3D Modelling to Provide Smart Monitoring of Road Pavement Conditions. *Information* **2020**, *11*, 568. [CrossRef]
19. Luan, B.; Zhou, W.; Ao, Z.; Han, Z.; Xiao, Y. Fuel-Efficient Road Classification Methodology for Sustainable Open Pit Mining. *Appl. Sci.* **2025**, *15*, 6309. [CrossRef]
20. Zhang, Y.; Dou, X.; Zhao, H.; Xue, Y.; Liang, J. Safety Risk Assessment of Low-Volume Road Segments on the Tibetan Plateau Using UAV LiDAR Data. *Sustainability* **2023**, *15*, 11443. [CrossRef]
21. Lei, T.; Mohamed, A.; Claudel, C. An IMU-Based Traffic and Road Condition Monitoring System. *HardwareX* **2018**, *4*, e00045. [CrossRef]
22. Ajayi, O.O.; Kurien, A.M.; Djouani, K.; Dieng, L. Analysis of Road Roughness and Driver Comfort in Long-Haul Road Transportation Using Random Forest Approach. *Sensors* **2024**, *24*, 6115. [CrossRef] [PubMed]
23. Alqaydi, S.A.; Zeiada, W.; El Wakil, A.; Alnaqbi, A.J.; Azam, A. A Comprehensive Review of Smartphone and Other Device-Based Technologies for Road Surface Condition Monitoring. *Eng* **2024**, *5*, 3397–3426. [CrossRef]
24. Shishkin, P.V.; Malozyomov, B.V.; Martyushev, N.V.; Sorokova, S.N.; Efremenkov, E.A.; Valuev, D.V.; Qi, M. Mathematical Logic Model for Analysing the Controllability of Mining Equipment. *Mathematics* **2024**, *12*, 1660. [CrossRef]
25. Yu, Q.; Fang, Y.; Wix, R. Evaluation Framework for Smartphone-Based Road Roughness Index Estimation Systems. *Int. J. Pavement Eng.* **2023**, *24*, 2183402. [CrossRef]
26. Janani, L.; Doley, R.; Sunitha, V.; Mathew, S. Precision Enhancement of Smartphone Sensor-Based Pavement Roughness Estimation by Standardizing Host Vehicle Speed. *Can. J. Civ. Eng.* **2022**, *49*, 716–730. [CrossRef]
27. Haja Mohideen, A.J.; Rosli, M.F.; Mohamad Hanif, N.H.H.; Mohd Zaki, H.F.; Husman, M.A.; Muthalif, A.G.A.; Kumar, D. Pavement Condition Analysis via Vehicle Mounted Accelerometer Data. *IIUM Eng. J.* **2020**, *21*, 73–84. [CrossRef]
28. Kumar, P.; Angelats, E. An Automated Road Roughness Detection from Mobile Laser Scanning Data. *Int. Arch. Photogramm. Remote Sens. Spat. Inf. Sci.* **2017**, *XLII-1/W1*, 91–96. [CrossRef]
29. Kopsiaftis, G.; Katsamenis, I.; Rallis, I.; Bakalos, N.; Zafeiropoulos, C.; Georgoulas, I.; Kourtis, I.; Kavouras, I.; Markoulidakis, I.; Karolou, E.E.; et al. IKAROS: A UAV-Based Integrated System for Monitoring Road Defects and Managing Vehicle Traffic and Emergencies on Road Transport Networks. In *PETRA '24: Proceedings of the 17th ACM International Conference on PErvasive Technologies Related to Assistive Environments*; Association for Computing Machinery: New York, NY, USA, 2024; pp. 1–7. [CrossRef]
30. Al-Sabaeei, A.M.; Souliman, M.I.; Jagadeesh, P. Smartphone Applications for Pavement Condition Monitoring: A Review. *Constr. Build. Mater.* **2024**, *410*, 134207. [CrossRef]
31. Golbasi, O.; Kina, E. Haul Truck Fuel Consumption Modeling under Random Operating Conditions: A Case Study. *Transp. Res. Part D Transp. Environ.* **2022**, *102*, 103135. [CrossRef]
32. Samie, M.; Golroo, A.; Tavakoli, D.; Fahmani, M. Potential Applications of Connected Vehicles in Pavement Condition Evaluation: A Brief Review. *Road Mater. Pavement Des.* **2024**, *25*, 889–913. [CrossRef]
33. Mahlberg, J.A.; Li, H.; Zachrisson, B.; Leslie, D.K.; Bullock, D.M. Pavement Quality Evaluation Using Connected Vehicle Data. *Sensors* **2022**, *22*, 9109. [CrossRef] [PubMed]
34. Mahlberg, J.A.; Li, H.; Zachrisson, B.; Mathew, J.K.; Bullock, D.M. Applications of Using Connected Vehicle Data for Pavement Quality Analysis. *Front. Future Transp.* **2024**, *4*, 1239744. [CrossRef]

35. Thompson, J.A.; Desai, M.; Bullock, D.M. Evaluation of Connected Vehicle Pavement Roughness Data for Statewide Needs Assessment. *Infrastructures* **2025**, *10*, 248. [CrossRef]
36. Thompson, J.A.; Desai, M.; Bullock, D.M. A Comparison of Connected-Vehicle Roughness and Traditional Pavement Condition Index. *Future Transp.* **2026**, *6*, 47. [CrossRef]
37. Jeong, J.; Jo, H. Toward Real-World Implementation of Deep Learning for Smartphone-Crowdsourced Pavement Condition Assessment. *IEEE Internet Things J.* **2024**, *11*, 6328–6337. [CrossRef]
38. Azhar, K.; Murtaza, F.; Yousaf, M.H.; Habib, H.A. Computer Vision Based Detection and Localization of Potholes in Asphalt Pavement Images. In *Proceedings of the 2016 IEEE Canadian Conference on Electrical and Computer Engineering*; IEEE: Piscataway, NJ, USA, 2016; pp. 1–5. [CrossRef]
39. Anand, S.; Gupta, S.; Darbari, V.; Kohli, S. Crack-Pot: Autonomous Road Crack and Pothole Detection. In *Proceedings of the 2018 Digital Image Computing: Techniques and Applications*; IEEE: Piscataway, NJ, USA, 2018; pp. 1–8. [CrossRef]
40. Chaowasakoo, P.; Seppälä, H.; Koivo, H.; Zhou, Q. Digitalization of Mine Operations: Scenarios to Benefit in Real-Time Truck Dispatching. *Int. J. Min. Sci. Technol.* **2017**, *27*, 229–236. [CrossRef]
41. Moradi Afrapoli, A.; Askari-Nasab, H. Mining Fleet Management Systems: A Review of Models and Algorithms. *Int. J. Min. Reclam. Environ.* **2019**, *33*, 42–60. [CrossRef]
42. Moradi Afrapoli, A.; Tabesh, M.; Askari-Nasab, H. A Stochastic Hybrid Simulation-Optimization Approach toward Haul Fleet Sizing in Surface Mines. *Min. Technol.* **2019**, *128*, 61–76. [CrossRef]
43. Moradi Afrapoli, A.; Tabesh, M.; Askari-Nasab, H. A Multiple Objective Transportation Problem Approach to Dynamic Truck Dispatching in Surface Mines. *Eur. J. Oper. Res.* **2019**, *276*, 331–342. [CrossRef]
44. Blom, M.L.; Pearce, A.R.; Stuckey, P.J. Short-Term Planning for Open Pit Mines: A Review. *Int. J. Min. Reclam. Environ.* **2019**, *33*, 318–339. [CrossRef]
45. Shishkin, P.V.; Malozyomov, B.V.; Martyushev, N.V.; Kondratiev, V.V.; Dorofeev, E.M.; Kononenko, R.V.; Vit'kina, G.Y. Optimization of Energy Balance and Powertrain for Electric Mining Dump Trucks in Coal Mine Reclamation Operations. *World Electr. Veh. J.* **2025**, *16*, 601. [CrossRef]
46. Yeganejou, M.; Badiozamani, M.; Moradi-Afrapoli, A.; Askari-Nasab, H. Integration of Simulation and Dispatch Modelling to Predict Fleet Productivity: An Open-Pit Mining Case. *Min. Technol.* **2022**, *131*, 67–79. [CrossRef]
47. Li, N.; Feng, S.; Ye, H.; Wang, Q.; Jia, M.; Wang, L.; Zhao, S.; Chen, D. Dispatch Optimization Model for Haulage Equipment of Underground Mines. *Metals* **2021**, *11*, 1848. [CrossRef]
48. Peng, J.; Jiao, R.J.; Zhang, F. Machine Learning-Powered Dynamic Fleet Routing for Fuel-Efficient Transportation Systems. *Systems* **2025**, *13*, 1033. [CrossRef]
49. Tadubana, G.; Sigweni, B.; Suglo, R. Case-Based Reasoning System for Prediction of Fuel Consumption by Haulage Trucks in Open-Pit Mines. *Int. J. Electr. Comput. Eng.* **2021**, *11*, 3129–3136. [CrossRef]
50. van Dinter, R.; Tekinerdogan, B.; Catal, C. Predictive Maintenance Using Digital Twins: A Systematic Literature Review. *Inf. Softw. Technol.* **2022**, *151*, 107008. [CrossRef]
51. Martyushev, N.V.; Malozyomov, B.V.; Demin, A.Y.; Pogrebnoy, A.V.; Kurdyumov, G.E.; Kondratiev, V.V.; Karlina, A.I. Comparative Assessment of the Reliability of Non-Recoverable Subsystems of Mining Electronic Equipment Using Various Computational Methods. *Mathematics* **2026**, *14*, 723. [CrossRef]
52. Malozyomov, B.V.; Martyushev, N.V.; Babyr, N.V.; Pogrebnoy, A.V.; Efremenkov, E.A.; Valuev, D.V.; Boltrushevich, A.E. Modelling of Reliability Indicators of a Mining Plant. *Mathematics* **2024**, *12*, 2842. [CrossRef]
53. Kukushkin, I.; Ryabov, Y.; Borovkov, A. Digital Twins: A Systematic Literature Review Based on Data Analysis and Topic Modeling. *Data* **2022**, *7*, 173. [CrossRef]
54. Nobahar, P.; Xu, C.; Dowd, P.; Shirani Faradonbeh, R. Exploring Digital Twin Systems in Mining Operations: A Review. *Green Smart Min. Eng.* **2024**, *1*, 474–492. [CrossRef]
55. Rojas, L.; Peña, Á.; Garcia, J. AI-Driven Predictive Maintenance in Mining: A Systematic Literature Review on Fault Detection, Digital Twins, and Intelligent Asset Management. *Appl. Sci.* **2025**, *15*, 3337. [CrossRef]
56. Shakenov, A.; Sładkowski, A.; Stolpovskikh, I. Haul Road Condition Impact on Tire Life of Mining Dump Truck. *Nauk. Visnyk Natsionalnoho Hirnychoho Univ.* **2022**, *6*, 25–31. [CrossRef]
57. Dudek, M.; Dworzak, M.; Biessikirski, A. Influence of Blasting Approaches in In-Pit Haul Road Construction on Emission Levels and Resource Management: A Case Study from the Holcim "Dubie" Open-Pit Mine. *Appl. Sci.* **2025**, *15*, 12310. [CrossRef]
58. Liu, C.; Szirányi, T. Road Condition Detection and Emergency Rescue Recognition Using On-Board UAV in the Wildness. *Remote Sens.* **2022**, *14*, 4355. [CrossRef]
59. Hazrathosseini, A.; Moradi Afrapoli, A. Transition to Intelligent Fleet Management Systems in Open Pit Mines: A Critical Review on Application of Reinforcement-Learning-Based Systems. *Min. Technol.* **2024**, *133*, 50–73. [CrossRef]

60. Kaliyev, B.; Myrzakhmetov, B.; Mauletbekova, B.; Akhymbayeva, B.; Mashatayeva, G.; Merkibayev, Y.; Golik, V.I.; Malozyomov, B.V. Energy-Efficient and Reliable Hydrodynamic Separation of Spent Drilling Fluids: Experiments, Modeling, and Process Stability. *Energies* **2026**, *19*, 1659. [CrossRef]
61. Mahlberg, J.A.; Sakhare, R.S.; Li, H.; Mathew, J.K.; Bullock, D.M.; Surnilla, G.C. Prioritizing Roadway Pavement Marking Maintenance Using Lane Keep Assist Sensor Data. *Sensors* **2021**, *21*, 6014. [CrossRef] [PubMed]
62. Mahlberg, J.A.; Li, H.; Cheng, Y.-T.; Habib, A.; Bullock, D.M. Measuring Roadway Lane Widths Using Connected Vehicle Sensor Data. *Sensors* **2022**, *22*, 7187. [CrossRef] [PubMed]
63. Oliveira, H.; Correia, P.L. Automatic Road Crack Detection and Characterization. *IEEE Trans. Intell. Transp. Syst.* **2013**, *14*, 155–168. [CrossRef]
64. Zhang, L.; Yang, F.; Zhang, Y.D.; Zhu, Y.J. Road Crack Detection Using Deep Convolutional Neural Network. In *Proceedings of the 2016 IEEE International Conference on Image Processing*; IEEE: Piscataway, NJ, USA, 2016; pp. 3708–3712. [CrossRef]
65. Nakousi, C.; Pascual, R.; Anani, A.; Kristjanpoller, F.; Lillo, P. An Asset-Management Oriented Methodology for Mine Haul-Fleet Usage Scheduling. *Reliab. Eng. Syst. Saf.* **2018**, *180*, 336–344. [CrossRef]
66. Hazrathosseini, A.; Moradi Afrapoli, A. An Intelligent Rule-Based Decision-Making System for Preliminary Truck Dispatching within Open-Pit Mines. *Min. Technol.* **2025**, *134*, 3–14. [CrossRef]
67. Yu, Z.; Feng, H.; Meng, Y.; Xu, E.; Wu, Y. Braking energy management strategy for electric vehicles based on working condition prediction. *AIP Adv.* **2022**, *12*, 015220. [CrossRef]
68. Kunkyin-Saadaari, F.; Gyebuni, R.; Asamoah-Danquah, C. Supervisor-Field Engineering Approach (S-FEA) of Determining Tyre Failures in the Haul Trucks at Newmont Ahafo Mine. *Eng. Appl. Sci.* **2024**, *9*, 20–34. [CrossRef]
69. Kristjanpoller, F.; Viveros, P.; Zio, E.; Pascual, R.; Aranda, O. Equivalent Availability Index for the Performance Measurement of Haul Truck Fleets. *Eksploat. Niezawodn.* **2020**, *22*, 655–664. [CrossRef]
70. Alabbad, S.; Altınkaya, H. An Intelligent Predictive Maintenance Architecture for Substation Automation: Real-World Validation of a Digital Twin and AI Framework for Predictive Maintenance in Critical Infrastructure. *Electronics* **2026**, *15*, 416. [CrossRef]

Disclaimer/Publisher's Note: The statements, opinions and data contained in all publications are solely those of the individual author(s) and contributor(s) and not of MDPI and/or the editor(s). MDPI and/or the editor(s) disclaim responsibility for any injury to people or property resulting from any ideas, methods, instructions or products referred to in the content.